Review/Synthèse

Triangular antiferromagnets

M.F. Collins and O.A. Petrenko

Abstract: In this article we review the effects of magnetic frustration in the stacked triangular lattice. Frustration increases the degeneracy of the ground state, giving rise to different physics. In particular it leads to unique phase diagrams with multicritical points and novel critical phenomena. We describe the confrontation of theory and experiment for a number of systems with differing magnetic Hamiltonians; Heisenberg, Heisenberg with easy-axis anisotropy, Heisenberg with easy-plane anisotropy, Ising, and singlet ground state. Interestingly each leads to different magnetic properties and phase diagrams. We also describe the effects of ferromagnetic, rather than antiferromagnetic, stacking and of small distortions of the triangular lattice.

Résumé: Nous passons en revue les effets de la frustration magnétique dans un réseau triangulaire empilé. La frustration augmente la dégénérescence du fondamental, donnant naissance à une physique différente. En particulier, on observe des diagrammes de phase uniques avec des points multicritiques ainsi que de nouveaux phénomènes critiques. Nous comparons les résultats théoriques et expérimentaux pour un certain nombre de systèmes identifiés par leur Hamiltonien magnétique : Heisenberg, Heisenberg avec anisotropie axiale, Heisenberg avec anisotropie planaire, Ising et fondamental singulet. Il est intéressant de noter qu'ils mènent tous à des propriétés magnétiques et des diagrammes de phase différents. Nous décrivons aussi les conséquences pour le réseau triangulaire des effets de ferromagnétisme plutôt que d'antiferromagnétisme, de l'empilement et des petites distorsions du réseau. [Traduit par la rédaction]

1. Introduction

Although very few magnetic systems can be solved exactly in three dimensions, there is a reasonable understanding of the physics of simple systems without competing interactions. Numerical estimates for physical quantities exist to at least the accuracy that experiments currently attain. Many systems do exhibit competing interactions however, that is, interactions that do not all favour the same ordered state. Sufficiently strong competition can lead to new physics that is manifested by the appearance of noncolinear ordering, novel critical exponents, rich phase diagrams, or an absence of long-range order at low temperatures.

There are several ways in which frustration can arise. In this article attention is limited to geometric frustration arising from triangular arrangements of magnetic moments with each pair coupled antiferromagnetically. Figure 1a shows such a situation with three atoms forming an equilateral triangle. Atoms 1 and 2 form a state of lowest energy when their moments are aligned antiparallel, but

Received September 11, 1996. Accepted February 12, 1997.

M.F. Collins. Department of Physics and Astronomy, McMaster University, Hamilton, ON L8S 4M1, Canada; **Telephone:** (905) 529-7070 ext. 24172; **FAX:** (905) 546-1252; **e-mail:** mcollins@mcmail.cis.mcmaster.ca
O.A. Petrenko. Department of Physics, University of Warwick, Coventry, CV4 7AL, United Kingdom; **Telephone:** +44(1203)523-414; **FAX:** +44 (1203) 692-016; **e-mail:** phsby@csv.warwick.ac.uk

Fig. 1. Geometric frustration in the triangular antiferromagnet (a) Geometric frustration arising from triangular arrangements of magnetic moments with each pair coupled antiferromagnetically. (b) and (c) two degenerate solutions for the lowest energy of the system for a given spin vector at atom 1.

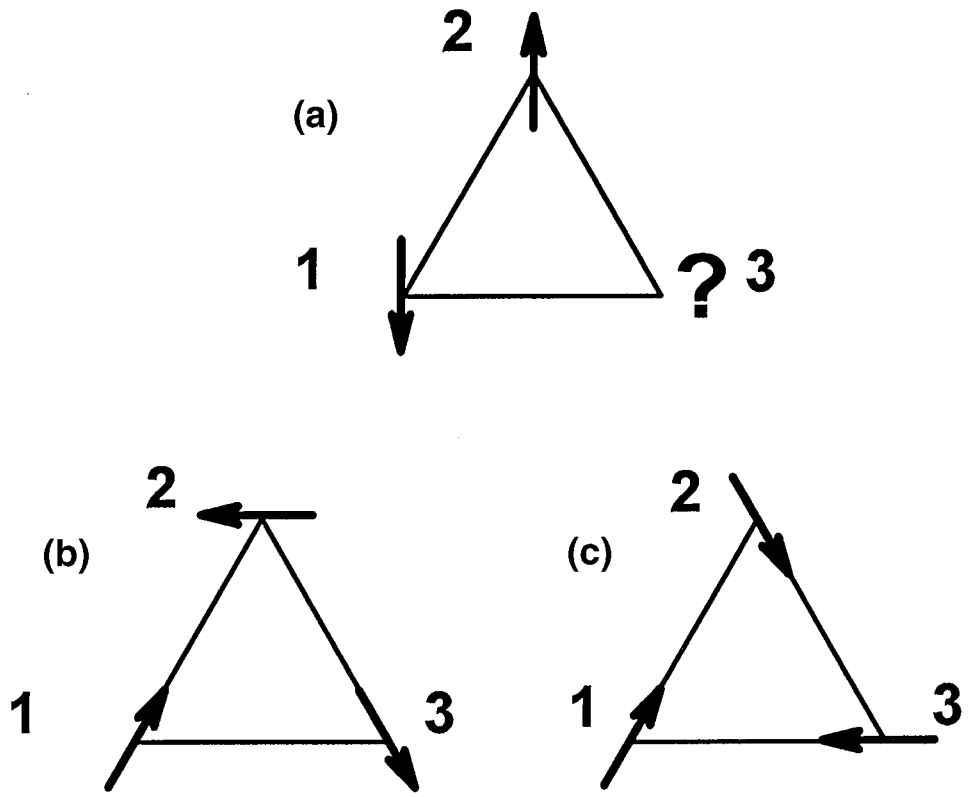

then atom 3 cannot align itself simultaneously antiparallel to the moment on both atoms 1 and 2, so it is frustrated. This frustration is most severe for an Ising system where spins can align only in one direction. For classical vector spins confined to the plane of the paper (XY interactions) there are two degenerate solutions for the lowest energy of the system for a given spin vector at atom 1. These are shown in Figs. $1b$ and $1c$. Both have the three spin vectors at $120°$ to each other, and the degeneracy corresponds to two different chiral states. The overall degeneracy of the ground state involves the product of this state and orientation of spin 1 in the plane; this corresponds to the group $Z_2 \times S_1$. For three-dimensional vector spins and isotropic Heisenberg interactions the degeneracy is greater still since the spin on atom 1 can be in any direction and then the spins on atoms 2 and 3 can be in any plane that contains the direction of spin 1. This degeneracy corresponds to the group SO(3). If the Hamiltonian has easy axis anisotropy, the plane of the three spins will contain the z axis and the angle between the three spin vectors will no longer be 120°. A general feature of these frustrated systems is that the ground state has extra degeneracy over and above that found in the analogous nonfrustrated systems. This is what gives rises to the possibility of new physics.

There are several ways that triangles of antiferromagnetic interactions can be built into a crystal lattice. In this article we limit consideration to the effects of frustration in the stacked triangular lattice. This is a lattice containing two-dimensional triangular sheets coupled by antiferromagnetic interactions J', with the sheets stacked perpendicular to the plane with coupling J between neighbouring atoms

Fig. 2. Crystal structure of (a) ABX_3 and (b) BX_2 compounds. A is an alkali metal, B is a transition metal, and X is a halogen atom.

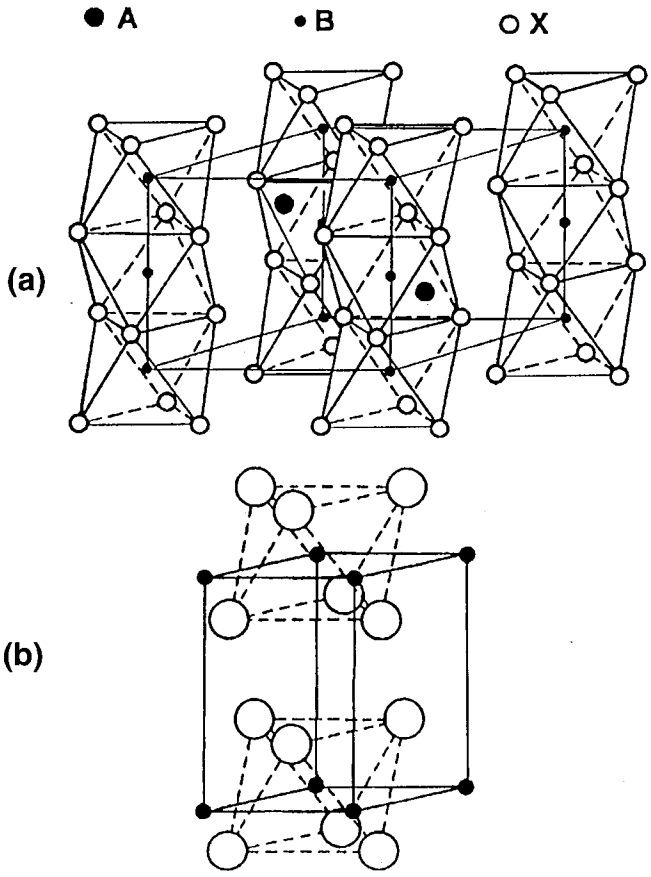

in different planes. Almost all the work on this lattice involves one of two crystal structures, one with composition ABX_3 where A is an alkali metal, B is a transition metal, and X is a halogen atom, and the other with composition BX_2. The crystal structure of these materials is shown in Fig. 2. In ABX_3 compounds there are chains of magnetic B atoms along the z direction coupled by superexchange interactions through three equivalent anions X. There is no direct superexchange coupling between atoms on neighbouring chains. The magnitude of the interplanar interactions J is typically two to three orders of magnitude greater than intraplanar interactions J', so that at high temperatures the magnetic properties become quasi one dimensional. In BX_2 compounds the strong superexchange coupling is intraplanar and the ratio of the magnitude of the interactions is reversed. At high temperatures the magnetic properties are quasi two dimensional. In a third known type of triangular antiferromagnets, ABO_2 compounds, the stacking of two-dimensional triangular sheets along the z direction is different from ABX_3 and BX_2 compounds, the stacking sequence is rhombohedral of the ABCABCABC... type. The crystal structure dictates the strong two-dimensional character of the magnetic system in ABO_2 compounds: the exchange path of the interplane interaction J', B–O–A–O–B, is much longer than that of the intraplane interaction J, B–B and B–O–B. At low temperatures almost all materials mentioned above form three-dimensional ordered magnetic structures that indicate the presence of magnetic frustration in the triangular lattice. In many, though not all, cases the low-temperature

Fig. 3. The stacked triangular antiferromagnet lattice.

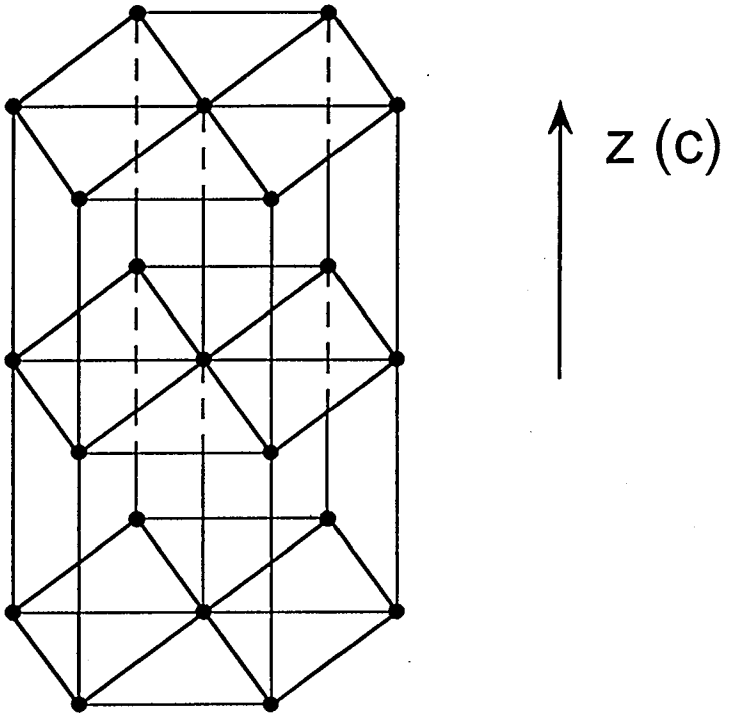

structure is built from one of the structures shown in Fig. 1.

Kawamura [1, 2] predicts that the extra degeneracy in the ground state of triangular antiferromagnets leads to new physics, which can be described in terms of universality classes based on the symmetry of the order parameter. Monte Carlo work [3–6] supports Kawamura's prediction for Heisenberg symmetry as does 4-ϵ renormalization group calculations [7]. However, the nonlinear σ model in 2+ϵ dimensions [8] indicates nonuniversal behaviour, likely with mean-field tricritical exponents, and the 3D renormalization group calculations with a resummation technique show a first-order phase transition [9]. The situation is no less clear for XY symmetry.

Experimentally stacked triangular antiferromagnets are found to have critical phase transitions with critical exponents that do not correspond to any of the standard universality classes for both Heisenberg [10] and XY [11] symmetry. In fact the critical points are found to be tetracritical in character [12] so that they clearly cannot belong in the same universality class as unfrustrated systems. This shows that the physics of magnetic systems can be changed by frustration. Both experiment and theory indicate that the ordered states found at low temperatures in frustrated systems have reduced ordered moments. Any detailed theory must therefore include quantum effects in determining the ground state, and classical theory may be substantially in error.

In fact much of the physics of the stacked triangular lattice is similar to that predicted for the two-dimensional triangular lattice [13–15] and the presence of the third dimension is not an essential ingredient of most of the ideas that are used in the field. However, for all well-characterized materials that have triangular magnetic lattices, the long-range order at low temperatures is three-dimensional in nature. For nearest-neighbour ferromagnetic or antiferromagnetic interactions, there is no extra

Table 1. Magnetic structure of ABX_3 triangular compounds.

A:B	Co	Cu	Fe	Mn	Ni	V	**X**
Rb	Ising [27]	nonhex [28]	F or SGS [29]	nontr [30]	HEA [31]	HEP [32]	Cl
Cs	Ising [33]	F [34]	SGS [29]	nontr [35]	HEA [36]	HEP [32]	
Rb	Ising [37]	—	HEP or SGS [38]	HEP [39]	HEA [40]	HEP [32]	Br
Cs	Ising [41]	—	SGS [42]	HEP [43]	HEA [44]	HEP [32]	
Rb	—	—	—	—	—	HEP [45]	I
Cs	—	—	HEP or SGS [46]	HEA [47]	⋆	HEP [32]	

$KNiCl_3$ HEP [48,49], $CsNiF_3$ F [50].
Ising Ising antiferromagnet.
HEP Heisenberg triangular antiferromagnet with easy-plane type anisotropy.
HEA Heisenberg triangular antiferromagnet with easy-axis type anisotropy.
SGS singlet-ground-state magnet.
F triangular antiferromagnet stacked ferromagnetically.
nontr magnetic structure is nontriangular.
nonhex crystal structure is nonhexagonal.
⋆ $CsNiI_3$ is reported to be not a localized spin system, but an itinerant electron system [51].

frustration involved by going to three dimensions, and the main influence of the presence of the third dimension is that the two-dimensional-ordering process is stabilized.

In this article we describe in some detail the magnetic properties of materials with stacked triangular lattices, paying special attention to cases where there are novel physical phenomena absent in the unfrustrated case. Emphasis is placed on the experimental results, though where possible the discussion is put in the appropriate theoretical context. Additional information about triangular antiferromagnets may be found in the related reviews [16–19]. We classify the stacked triangular lattice materials by the nature of the magnetic Hamiltonian. Section 2 describes materials with Heisenberg interactions, Sect. 3 describes systems with Ising Hamiltonians, Sect. 4 describes singlet-ground-state magnets, and Sect. 5 considers cases with ferromagnetic stacking of the planes. Section 6 describes magnetic properties of the diluted triangular antiferromagnets. Section 7 presents conclusions from these studies.

We conclude this section by listing the materials that have been studied in the context of stacked triangular antiferromagnetism.

(i) Table 1 shows the magnetic structure of ABX_3 triangular compounds. The cases where B is a chromium atom or A is a thallium atom are omitted since these compounds do not form with a triangular lattice compounds.

(ii) Four BX_2 compounds have been studied: VCl_2 and VBr_2 are close to Heisenberg systems [10], though there is weak easy-axis anisotropy, the magnetic structure of VI_2 is not clear [20,21]. $MnBr_2$ has a complex magnetic structure which is not triangular in nature [22].

(iii) Among ABO_2 compounds magnetic properties of only three triangular antiferromagnets have been investigated in details. $LiCrO_2$ and $CuCrO_2$ demostrate 120° magnetic structure with weak easy-axis anisotropy [23–25], $AgCrO_2$ has slightly modulated 120° structure [26].

2. Heisenberg triangular antiferromagnets

The stacked triangular magnetic lattice is shown in Fig. 3. Its magnetic properties for Heisenberg-type antiferromagnetism with single-ion anisotropy can be described on the basis of the following Hamiltonian:

$$\hat{\mathcal{H}} = J \sum_{i,j}^{\text{chains}} \boldsymbol{S}_i \boldsymbol{S}_j + J' \sum_{k,l}^{\text{planes}} \boldsymbol{S}_k \boldsymbol{S}_l + D \sum_i (S_i^z)^2 - g\mu_{\text{B}} \boldsymbol{H} \sum_i \boldsymbol{S}_i \tag{1}$$

Table 2. Exchange and anisotropy constants for triangular Heisenberg antiferromagnets.

	J (GHz)	J' (GHz) or J' and J'_1	D (GHz)
$CsNiCl_3$ $S=1$	345(8)–NS [52] 275–M [53]	6.0(6)–NS [52] 8(1)–ESR [54] 5.4–NS [55]	−13.0(1.5)–NS [52] −1.2–ESR [54]
$RbNiCl_3$ $S=1$	485–NS [56] 496–NS [58]	14–NS [56] 38(4)–ESR [59]	−1.5–ESR [57] −1.0(1)–ESR [59]
$RbNiBr_3$	520–ESR [60]	21–M [40]	—
$CsNiBr_3$ $S=1$	354–M [44]	6.5–NMR [61]	−13.5–NMR [61] −31.2–M [44]
$CsMnI_3$ $S=5/2$	198(2)–NS [62]	1.0(1)–NS [62] 0.9–NS [63] 0.88–NS [65]	−0.50(2)–NS [62] −1.7–NS [64] −1.07–ESR [66]
$CsMnBr_3$ $S=5/2$	211(2)–NS [67] 215(3)–NS [69]	0.46(5)–NS [68] 0.41(2)–NS [69] 0.46–NS [70]	3.4(5)–NS [68] 2.9(3)–NS [69] 2.9–NS [70]
$RbMnBr_3^\star$ $S=5/2$	199–NS [71] 186–M [72]	0.54–NS [71] 0.22–M [72]	2.2–NS [71] 1.3–M [72]
$KNiCl_3^\star$ $S=1$	310(6)–NS [49] 312–M [48]	0.23 and 0.27–ESR [48]	130(10)–NS [49] 18–M [48]
$CsVBr_3$ $S=3/2$	1700–NS [73] 1700-1900–M [73]	0.43–NS [74]	0.48–NS [74]
$RbVBr_3$ $S=3/2$	2700–NS [75]	J' and $1.7J'$–NS [76]	—
$CsVCl_3$ $S=3/2$	2400–NS [73] 3500–NS [77] 2700–NS [78] 2400–M [73]	0.15–NS [74] 1.0–NS [77] 0.8–NS [55]	0.29–NS [74]
$CsVI_3$ $S=3/2$	1100–NS [73] 1100-1400–M [73]	1.9–NS [74]	3.4–NS [74]
VCl_2 $S=3/2$	2.8(1)–NS [10]	458(13)–NS [10] 480–M [79]	−1.5–NS [10] −2–ESR [80]
VBr_2 $S=3/2$	4–NS [81]	333–NS [81] 333–M [79]	−2–ESR [80]
VI_2 $S=3/2$	—	125–M [79]	—
$LiCrO_2$ $S=3/2$	—	810–M [82] 780–ESR [83]	—
$CuCrO_2$ $S=3/2$	—	236–M [84]	—
$AgCrO_2$ $S=3/2$	—	186–M [84]	—

NS, neutron-scattering measurements
ESR, electron spin resonance measurements
NMR, nuclear magnetic resonance measurements
M, magnetization and susceptibility measurements

In the literature a variety of units are used for quantities listed in Table 2. The conversion factors are 1 GHz = 4.136 μeV = 0.0480 K = 0.03336 cm^{-1}.

* Data for $RbMnBr_3$ and $KNiCl_3$ refer to orthorhombic and hexagonal phases, respectively.

where $\boldsymbol{S}$ is a spin of the magnetic ion; J is the exchange integral along the c axis of the crystal; J' is the exchange integral in the perpendicular direction; and D is the anisotropy constant, whose sign determines the orientation of the spin plane relative to the crystal axes. The first sum describes the exchange energy along the chain, the second sum describes the exchange energy in the basal plane, and the third and fourth sums represent the single-ion anisotropy energy and the Zeeman energy of the spins in a external magnetic field $\boldsymbol{H}$, respectively. The case $D = 0$ corresponds to a pure Heisenberg system. All real triangular magnets have nonzero D, but if $|D|$ is small compared with both $|J|$ and $|J'|$ the magnetic properties will be close to those of Heisenberg systems except at very low temperatures $T < DS^2$ or very close to the critical point. If $D > 0$ the ground state in zero field has spins confined to the xy plane and in the critical region the fluctuations will only diverge for spin components within the xy plane. If $D < 0$ the anisotropy energy will be minimized for spins aligned perpendicular to the xy plane. This term will compete with the antiferromagnetic J' exchange term and lead to additional frustration.

Table 2 lists the parameters J, J' (both assumed nearest-neighbour interactions only), and D that have been determined experimentally in units of frequency, or energy divided by h. The data confirm our previous observation that ABX_3 compounds are quasi-one-dimensional with $J \gg J'$ and that VX_2 compounds are quasi-two-dimensional with $J \ll J'$. In the ABO_2 compounds only the in-plane exchange, J' has been measured reliably.

2.1. Quasi-two-dimensional triangular antiferromagnets of type BX_2 and ABO_2

VCl_2 and VBr_2 crystallize in the CdI_2 structure with a space group $P\overline{3}m1$. VI_2 exists in two modifications, black and red. The black modification is composed of a statistical alternating layer structure of the CdI_2 and the $CdCl_2$ types, while the red modification crystallizes in the CdI_2-type structure [85]. This feature may explain the fact that the majority of work on VI_2 was done on powder, rather than on single crystal — it is difficult to prepare a good quality single crystal of VI_2.

VCl_2 and VBr_2 are important because they are the stacked triangular materials with Hamiltonians closest to the Heisenberg form. Both materials show critical phase transitions from ordered to paramagnetic states in zero field [10, 86, 87].

Despite numerous efforts to determine magnetic structures of BX_2 antiferromagnets, including NMR spectra and relaxation measurements [88], ESR measurements [80], and direct neutron-scattering measurements [10, 20, 21, 81, 89] there are still some open question about spin-structures. Neutron polarization analysis has shown that below T_N the spin structure of VCl_2 is the 120° structure in the ac-plane [10], while in the case of VBr_2 neutron-scattering results are consistent with both the 120° structure in the ac-plane and a partially disordered structure whose spins cant from the c axis by 45° [81,89]. VI_2 has only been looked at by neutron-scattering in powder form. Two neutron powder measurements [20, 21] give different patterns. Solution of the structure will probably need single-crystal data, the simple triangular structure is not observed. There are two phase transitions, a critical transition at 16.3 K and a first-order transition at 14.4 K [21].

VCl_2 has weak easy-axis anisotropy as is shown by the data in Table 2 and also by the splitting of the critical point from the single tetracritical point of the frustrated Heisenberg Hamiltonian into two ordinary critical transitions at $T_{N1} = 35.88(1)$ K and at $T_{N2} = 35.80(1)$ K in zero field [10]. This splitting of about one part in 450 will give rise to crossover behaviour in the critical region [90]. For reduced temperatures $t = (T - T_N)/T_N$ of magnitude more than about 1/450 above T_{N1} or below T_{N2} the critical behaviour will be that of the frustrated Heisenberg system. Nearer to T_{N1} or T_{N2} the critical behaviour will reflect the fact that the correlation length only diverges along the z direction, not in the xy plane, and will be different. Thus it is possible, in principle, to measure three sets of critical exponents in VCl_2, though in practice only the Heisenberg exponents for $|t| > 1/450$ have been measured. In VBr_2 the splitting of $T_N = 28.66(2)$ K is even smaller and has not been observed [87]. The measured critical exponents should correspond to those of the frustrated Heisenberg system.

Table 3. Experimental values of critical exponents for frustrated Heisenberg systems, compared with three models.

Exponent	VCl_2	VBr_2	SO(3) [17]	Tricritical	Heisenberg [17]
β	0.20(2) [10]	0.20 [98]	0.30(2)	0.25	0.368(4)
ν	0.62(5) [10]	—	0.59(2)	0.5	0.710(7)
γ	1.05(3) [10]	—	1.17(2)	1.0	1.390(10)
α	—	0.30(5) [87]	0.24(8)	0.5	$-0.126(11)$
		0.59(5) and 0.28(2) [86]			

Table 3 lists the observed critical exponents in VCl_2 and VBr_2 and compares them with theoretical predictions. It is clear that the frustrated Heisenberg system has critical exponents that are far from those of the unfrustrated system, confirming that frustration changes the physics. Neither the SO(3) nor tricritical model are in complete accord with experiment; the SO(3) model is in disagreement with experiment for β and γ and the tricritical exponents are in disagreement for ν and α. In every case both these models are significantly better than the unfrustrated Heisenberg model.

$MnBr_2$ also does not order in the triangular structure. Its structure, based on single-crystal neutron data, is complex based on arrangements with two up spins followed by two down spins [22]. There are two magnetic phase transitions: second order at T_{N1} =2.32 K and first order at T_{N2} =2.17 K.

$LiCrO_2$ has been studied by single-crystal susceptibility and neutron-diffraction measurements [23, 24], optical measurements [91, 92], ESR [83, 93], and neutron-diffraction measurements [94] on a powder sample. Three-dimensional magnetic ordering, characterized by a double-$\boldsymbol{Q}$ 120° structure with nonequivalent wave vectors $\boldsymbol{Q}$ of $(\frac{1}{3}\frac{1}{3}0)$ and $(-\frac{2}{3}\frac{1}{3}\frac{1}{2})$ [24], is observed below the single-phase-transition temperature $T_N = 64$ K. Polarization analysis of neutron-scattering data shows that spin triangulars are confined in a plane including the c axis, that is, the magnetic anisotropy is of the easy-axis type. On the other hand, absence of splitting of T_N and of anisotropy in the susceptibility above T_N demonstrate that magnetic anisotropy D is much smaller than exchange interactions J and J'. No direct measurements of D and J' have been reported, the only attempt to estimate the J/J' ratio from the phase transition temperature was made by Angelov and Doumerc [95], which gives only a very rough estimate. The ratio J/J' could also be estimated from susceptibility measurements since it is proportional to the $(\chi_{\parallel c} - \chi_{\perp c})/\chi$ = 5% ratio (note the difference between $LiCrO_2$ and VX_2 compounds: in $LiCrO_2$ $\chi_{\parallel c} > \chi_{\perp c}$). The optical and ESR measurements were mostly devoted to the problem of finding of the characteristic point-defects known as Z_2 vortices, predicted theoretically by Kawamura and Miyashita [96]. It is believed the line width of the exciton magnon absorption [91] and EPR linewidth [93] exhibit Z_2-vortex-induced broadening.

The rest of the ABO_2-type triangular antiferromagnets have been studied only in a powder form. $AgCrO_2$ has been reported to order magnetically below 24 K. It forms a slightly modulated 120° structure [26] with magnetic peaks at (0.327 0.327 0). The width of peaks indicates that the development of the true long-range magnetic order is suppressed. Results of neutron powder-diffraction studies on $CuCrO_2$ below $T_N = (25 \pm 0.5)$ K are consistent with the 120° structure in the ac plane with moment $(3.1 \pm 0.2)\mu_B$ [25]. No long-range magnetic ordering has been found in $NaTiO_2$ and $LiNiO_2$ down to 1.4 K [97] and in $NaCrO_2$ and $KCrO_2$ down to 2 K [94].

An interesting issue is a magnetic moment reduction at low temperature. There are three general causes that effect the value of magnetic moments in ABX_3 and VX_2 compounds: (1) covalency reduction, (2) effect of frustration, and (3) quantum fluctuations enhanced by the low-dimensionality of the magnetic system. According to high-temperature susceptibility measurements [79], the moment of V^{2+} can be estimated as 3.96, 4.07, and 4.07 μ_B for VCl_2, VBr_2, and VI_2, respectively, suggesting small covalency reduction. From the low-temperature neutron-diffraction data an average moment in VCl_2 is $<S>/S = 0.80 \pm 0.06$ [10], and in VBr_2 $<S>/S = 0.83 \pm 0.04$ or $<S>/S = 1.02 \pm 0.05$ depending upon magnetic structure assumed [81]. The relatively small reduction of the magnetic

Fig. 4. Magnetic phase diagram of a Heisenberg triangular antiferromagnet with a small easy-axis anisotropy.

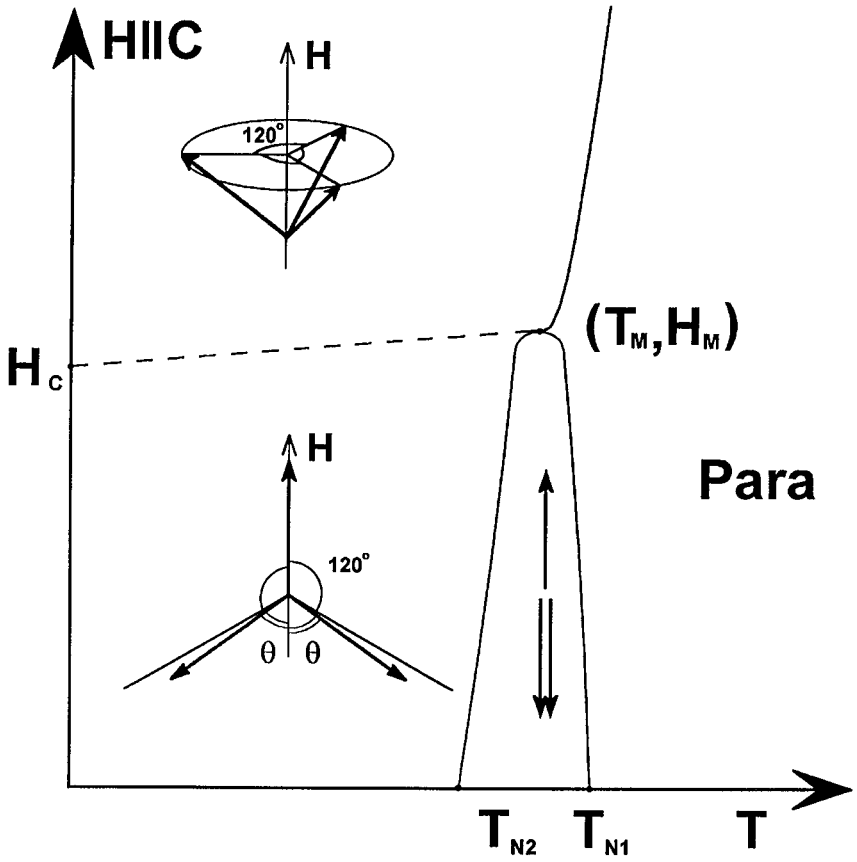

moment in the two-dimensional systems in comparison with almost 50% reduction in some ABX_3 one-dimensional systems (see Sect. 2.2) indicates dimensionality (quasi-two-dimensional rather than quasi-one-dimensional) and quantum fluctuations are the major influences on the moment reduction in the stacked triangular lattice. Note that, in theory, the average magnetic moment of a two-dimensional magnetic system is nonzero, while in a one-dimensional system $<S>= 0$.

2.2. Heisenberg triangular antiferromagnet with easy-axis anisotropy

In this section we describe materials with a Hamiltonian (1) that has an exchange term and a single-ion anisotropy with $D < 0$. This negative value of D makes it energetically favourable for the moments to align perpendicular to the ab plane. This breaks the isotropic symmetry of the Heisenberg Hamiltonian and leads to changes in the physics.

There are five materials with this Hamiltonian, all of composition ABX_3, with space group $P6_3/mmc$ and a stacked triangular lattice of spins. These are $CsNiCl_3$, $RbNiCl_3$, $CsNiBr_3$, $RbNiBr_3$, and $CsMnI_3$. All exhibit the quasi-one-dimensional behaviour typical of this crystal structure with the value of the exchange interaction, J, along c more than an order of magnitude greater than the intraplanar exchange interaction, J', and with the magnitude of D of the same order as that of J'. Experimental values of J, J', and D are given in Table 2. In all cases the exchange interaction is antiferromagnetic. In some cases there are major discrepancies between experimental results; we will look at this later in this section.

All five materials have a magnetic phase diagram as shown in Fig. 4. At low temperatures and magnetic fields the magnetic structure is observed to be the triangular structure with the c axis in the plane of the triangle. The anisotropy favours alignment of spins perpendicular to the basal plane resulting in structures where the angle θ in Fig. 4 is less than 60°. Each ab plane has a net moment perpendicular to it that can be observed by neutron diffraction. However, the planes are stacked antiferromagnetically because of the large antiferromagnet exchange interaction, J, along the chains. This results in the whole crystal being an antiferromagnet. For a classical system

$$\cos\ \theta = \frac{1}{2(1+\frac{D}{6J'})}, \qquad |D| < 3J' \quad \text{and} \quad D < 0 \tag{2}$$

At $|D| = 3J'$ the triangular structure collapses into a colinear structure with two spins along $+c$ and one spin along $-c$. The anisotropy is not large enough for this to happen in any of the materials considered in this section. Section 3 describes collapsed cases.

At a temperature T_{N2} there is a critical phase transition to the colinear structure as shown in Fig. 4. Thus for classical spins, as $|D|$ increases to $3J'$, T_{N2} decreases to zero. At a higher temperature, $T_{N1} > T_{N2}$, there is a second critical phase transition, this time to the paramagnetic state. The difference $(T_{N1} - T_{N2})/T_{N1}$ is a measure of the relative strength of the anisotropy, D, and the exchange, J'. The colinear structure is energy independent of the applied field, while for all competing structures the energy decreases as the field increases. Thus it becomes less stable as the field increases.

As a field is applied along the c axis at low temperature the angle θ changes in different directions for successive planes; in the plane shown in Fig. 4 the angle θ increases on application of a field along Z. At a field H_c there is a first-order phase transition to the canted structure shown in Fig. 4. In this structure the xy component of the moments form an equilateral triangle, while the Z components are aligned ferromagnetically along the field direction. For a classical system with J large compared with J' or $|D|$, Tanaka et al. [107] show that

$$(g\mu_B H_c)^2 = 16JDS^2 \tag{3}$$

at $T = 0$. It should be noted that the expression given in ref. 46 by Tanaka et al. differs from that given above by a factor of 2 because they define J to be half of our J.

There is a multicritical point at T_M, H_M where all four phases meet. Alternatively, this point can be described as the intersection of three lines of critical phase transitions and one line of first-order phase transitions. The experimentally determined parameters of the phase diagram, T_{N1}, T_{N2}, T_M, H_c, H_M, and θ are given in Table 4. There is reasonable agreement between different experimental measurements here, in contrast to the descrepancies noted between some of the measurements of the parameters of the Hamiltonian (Table 2).

Now that we have given an overview of the properties of materials with easy-axis anisotropy, we go back to examining the experimental values of the parameters in the Hamiltonian, and to checking consistency with phase-diagram parameters. One reason for inconsistency is that it is believed that the neutron-scattering values of -13.0 GHz for $CsNiCl_3$ and -0.5 GHz for $CsMnI_3$ are in error because of incorrect branch assignments. A second problem is that the resonance experiments actually measure H_c and then derive D from (3) and known values of J. Unfortunately the equation may not hold for $S = 1$. The difficulty arises from the need to incorporate quantum fluctuations into the theory. A well-established technique for taking these into account involves an expansion in powers of $1/(2S)$ [116,117]. Zhitomirsky and Zaliznyak [118] show that inclusion of this term in (3) yields a negative value for H_c^2. Although this is nonphysical, the result serves notice that (3) is not good for values of S as small as 1. Furthermore, the first term in the quantum correction for $S = 1$ renormalizes J by 18% and D by -50%. Most experiments will measure the renormalized values, not the bare values. A further difficulty with the nickel compounds is that because of their quasi-one-dimensional

Table 4. Characteristics of the Heisenberg triangular antiferromagnets with easy-axis anisotropy.

	T_{N1}, T_{N2} (K)	$T_{\rm M}$ (K)	$H_{\rm c}$ (T)	$H_{\rm M}$ (T)	$\theta_{T=0}$ ($^\circ$)	$\mu_{T=0}$ ($\mu_{\rm B}$)
$CsNiCl_3$	4.84, 4.40–NMR [99]	4.48–C [100]	1.99–M [101]	2.25–C [100]	59–NS [102]	1.1(1)–NS [103, 104]
$S = 1$	4.88(5), 4.40(5)–M [101]	4.495–US [105]	1.9–ESR [54, 106]	2.105–US [105]	50–ESR [107]	1.4(2)–NS [36]
	4.83(8), 4.46(8)–NS [52]	4.48–ESR [105]		2.13–ESR [105]	59-ESR [108]	
	4.80(1), 4.388(4)–US [109]					
$RbNiCl_3$	11.25, 11.11–NS [110]	11.8–M [101]	2.05–M [101]	2.65–M [101]	57.5–NS [31]	1.3(1)–NS [31]
$S = 1$			2.01–ESR [59]	2.4–ESR [59]		1.5(2)–NS [36]
$CsNiBr_3$	14.06, 11.51–NMR [61]	11.0–M [111]	8.8–M [111]	9.88–M [111]	39–NMR [61]	—
$S = 1$	14.25, 11.75–C [44]				58–ESR [108]	
	13.46, 11.07–B [112]					
$RbNiBr_3$	23.5, 21.47–ESR [60]	—	—	—	—	—
$S = 1$						
$CsMnI_3$	11.2, 8.17–NS [113]	8.85–M [111]	5.3–M [111]	5.95–M [111]	50(2)–NS [47]	3.7–NS [47]
$S = 5/2$	11.41, 8.21–NS [62]	9.02(5)–B [114]	5.4–M [47]	5.86(1)–B [114]	51(1)–NS [62]	
	11.20(1) 8.166(5)–NS [115]		5.2–ESR [66]		55-ESR [108]	

NS, neutron-scattering measurements.
ESR, electron spin resonance measurements.
NMR, nuclear magnetic resonance measurements.
M, magnetization and susceptibility measurements.
C, specific-heat measurements.
US, ultrasonic velocity and attenuation measurements.
B, birefringence measurements.

properties, there may be vestiges of the Haldane effect in their low-temperature properties. Of course a full quantum treatment will take this into account, but it may not be apparent in the first term of a $1/(2S)$ expansion. Several neutron-scattering experiments claim to see Haldane-gap effects in the three-dimensional ordered phase [52, 56, 65, 114, 119], and conventional spin-wave theory (i.e., spin-wave theory without quantum corrections) does not fit the measured dispersion relations. Without further theoretical guidance there must be some doubts about the reported values of J, J', and D for the nickel compounds even in cases where the experimental data are irreproachable. Affleck [120] has argued Haldane correlations will still be effective in the three dimensionally ordered phase. His treatment shows much better qualitative agreement with experiment than linear spin-wave theory and provides a theoretical underpinning for the claims that the experiments constitute solid confirmation of the existence of the Haldane gap. In large fields, $H > T_{\rm c}$ and $T_{\rm M}$, the quantum fluctuations are reduced [53, 121] and the interpretational difficulties are less severe.

In $CsMnI_3$ the quantum corrections are smaller; in leading order by a factor of 2.5 so that they are of the same order as the experimental uncertainties. The spin wave dispersion relations follow conventional spin wave theory [63,64]. The values of J, J', and D quoted in the table are the directly measured values without application of any quantum corrections.

It is interesting to consider the effects of increasing departures of the Hamiltonian from the Heisenberg form in easy-axis systems. This is equivalent to increasing $|D|$ while keeping the exchange parameters J and J' fixed. Even small values of $|D|$ break the symmetry by aligning the moments triangles in a plane that contains the z axis and splitting the critical point into two critical points at T_{N1} and T_{N2}. T_{N2} decreases until it becomes zero at $-D = 3J'$. T_{N1} and $T_{\rm M}$ increase as $|D|$ increases, as can be seen for instance by comparing $CsNiCl_3$ with $CsNiBr_3$ where J and J' are similar but the values of D differ by an order of magnitude. $H_{\rm c}$ increases as $|D|^{1/2}$ and experiment seems to indicate that $H_{\rm M} \simeq 1.1 H_{\rm c}$.

We now discuss the phase diagram and critical properties of the easy-axis magnets. The theory is constructed assuming that the parameters of the system are such as to give a phase diagram of the type shown in Fig. 4 with the magnetic structures that we have described. Thus antiferromagnetic Heisenberg interactions J and J' are taken on a stacked triangular lattice with easy-axis anisotropy $-D < 3J'$. Then, building on the ideas of the chiral universality classes described earlier, theory makes a number of predictions based on Landau-type theories, scaling, and renormalization group calculations.

1. There is a multicritical point connecting a line of first-order phase transitions and three lines of critical phase transitions [122].

2. All three lines of critical points come in tangentially to the first order spin-flop line [123].

3. The lines of phase transitions through T_{N1} and T_{N2} both follow the XY universality class [123].

4. The phase transition from the paramagnetic state to the spin flop state follows the chiral XY universality class [123].

5. At the multicritical point the phase transition should follow the chiral Heisenberg universality class [123].

6. The transition region around the multicritical point should not be large [124].

The first of these predictions is obeyed by all the materials studied in this section. The experimental evidence from the highest accuracy phase diagrams in $CsNiCl_3$ [105, 109], $CsNiBr_3$ [111], and $CsMnI_3$ [111, 114] suggests that the second prediction is also good. The experiments all clearly show that the two lines of phase transitions to paramagnetism come in parallel to the line of first-order phase transitions and give clear indications that there is curvature in the line of phase transitions through T_{N2} close to the multicritical point such as to make the predicted effect likely.

Table 5 lists the experimental determinations of the critical exponents β, ν, γ, and α and compares the results with predictions for various universality classes. As well as the critical exponents, Table 4

Table 5. Observed critical exponents for easy-axis materials and predicted critical exponents [114, 126] for various universality classes. Subscripts 1, 2, M, and F represent exponents at T_{N1}, T_{N2}, the multicritical point, and between the spin-flop and the paramagnetic phase, respectively.

Exponent	Material	Experimental value	Chiral XY	Chiral Heisenberg	XY	Heisenberg
β_1	$CsNiCl_3$	0.32(3) [99]	0.25(1)	0.30(2)	0.35	0.36
	$CsNiCl_3$	0.30(2) [102]				
	$RbNiCl_3$	0.27(1) [110]				
	$CsMnI_3$	0.32(1) [115]				
ν_1	$CsMnI_3$	0.59(3) [113]	0.54(2)	0.59(2)	0.669	0.705
γ_1	$CsMnI_3$	1.12(7) [113]	1.13(5)	1.17(7)	1.316	1.387
α_1	$CsNiCl_3$	$-0.05(8)$ [126]	0.34(6)	0.24(8)	-0.008	-0.116
$(A^+/A^-)_1$	$CsNiCl_3$	1.21(5) [126]	0.36(2)	0.54(2)	0.99	1.36
β_2	$CsNiCl_3$	0.32(3) [99]	0.25(1)	0.30(2)	0.35	0.36
	$CsNiCl_3$	0.30(2) [102]				
	$RbNiCl_3$	0.28(1) [110]				
	$CsMnI_3$	0.35(1) [115]				
ν_2	$CsMnI_3$	0.56(2) [113]	0.54(2)	0.59(2)	0.669	0.705
γ_2	$CsMnI_3$	1.04(3) [113]	1.13(5)	1.17(7)	1.316	1.387
α_2	$CsNiCl_3$	$-0.06(10)$ [126]	0.34(6)	0.24(8)	-0.008	-0.116
	$CsMnI_3$	$-0.05(15)$ [126]				
$(A^+/A^-)_2$	$CsNiCl_3$	1.2(3) [126]	0.36(2)	0.54(2)	0.99	1.36
	$CsMnI_3$	1.2 [126]				
β_M	$CsNiCl_3$	0.28(3) [125]	0.25(1)	0.30(1)	0.35	0.36
α_M	$CsNiCl_3$	0.25(8) [126]	0.34(6)	0.24(8)	-0.008	-0.116
	$CsNiCl_3$	0.23(4) [114]				
	$CsMnI_3$	0.28(6) [126]				
	$CsMnI_3$	0.44(3) [114]				
$(A^+/A^-)_M$	$CsNiCl_3$	0.52(10) [126]	0.36(2)	0.54(2)	0.99	1.36
	$CsMnI_3$	0.42(10) [126]				
β_F	$CsNiCl_3$	0.243 [125]	0.25(1)	0.30(2)	0.35	0.36
α_F	$CsNiCl_3$	0.37(8) [126]	0.34(6)	0.24(8)	-0.008	-0.116
	$CsNiCl_3$	0.342(5) [114]				
	$CsMnI_3$	0.34(6) [126]				
$(A^+/A^-)_F$	$CsNiCl_3$	0.30(11) [126]	0.36(2)	0.54(2)	0.99	1.36
	$CsMnI_3$	0.31(8) [126]				

also compares experiment and theory for the amplitude ratio, above and below T_N, of the specific-heat divergence.

Inspection of Table 4 shows that there is generally good agreement between experiment and theory for the specific-heat data, but that the agreement with the neutron data at $H = 0$ for β, γ, and ν is not good. Recent neutron measurements [125] for β at the multicritical point and for the spin-flop-to-paramagnetic phase transition agree well with theoretical predictions.

We conclude that theoretical predictions 1, 2, 4, and 5 above are confirmed by experiment. Prediction 6 has not been tested. Experiment does not bear out prediction 3 that the critical phase transitions at T_{N1} and T_{N2} follow the XY universality class. The measured indices do not fall within any standard universality class, but they do seem to be the same at the two transitions as predicted. The neutron data could be described numerically by chiral Heisenberg critical exponents,

Table 6. Characteristics of the Heisenberg triangular antiferromagnets with easy-plane type anisotropy.

	Ordering type	Space group at low T	T_N (K) or T_{N1} and T_{N2}, (K)	H_c (T)	$\mu_{T=0}$, (μ_B)
$CsMnBr_3$ $S=5/2$	$D>3J'$	$P6_3/mmc$	8.32–NS [12]	6.2–NS [12]	3.3–NS [43]
$CsVBr_3$ $S=3/2$	$D<3J'$	$P6_3/mmc$	20.4–NS [32] 20.3–M [127]	—	1.87–NS [32]
$CsVCl_3$ $S=3/2$	$D<3J'$	$P6_3/mmc$	13.8–NS [32]	—	1.97–NS [32]
$RbVCl_3$ $S=3/2$	$D<3J'$	$P6_3/mmc$	19(1)–NS [32]	—	2.31–NS [32]
$CsVI_3$ $S=3/2$	$D<3J'$	$P6_3/mmc$	34.8–NS [32] 32(1)–NS [45]	—	1.64–NS [32]
$RbMnBr_3$ $S=5/2$	Distorted	there are two phases: hexagonal ($\leq P6_3/mmc$) orthorhombic ($Pbcm$ or $Pca2_1$)	 10.0–NS [71] 8.5–NS [71]	 — 3.9–M [128], 4.0–NS [129]*	 — 3.6–NS [39]
$KNiCl_3$ $S=1$	Distorted	there are two phases: hexagonal ($\leq P6_3/mmc$) orthorhombic ($Pbcm$ or $Pca2_1$)	 8.6–M [49], NS [130] 12.5–NS [130]	 2.3–M [49], 1.8–ESR [48] — —	 — —
$RbVBr_3$ $S=3/2$	Distorted	$P6_3cm$ or $P\bar{3}c1$	28.1 and 21.0–M [127]	—	1.53–NS [32]
$RbVI_3$ $S=3/2$	Distorted	$P6_3cm$ or $P\bar{3}c1$	25–NS [32]	—	1.44-NS [32]
$RbTiI_3$ $S=1$	Distorted	$P6_3cm$ or $P\bar{3}c1$	<4.2-NS [45]	—	—

*In the orthorhombic phase of $RbMnBr_3$ beside transition from triangular (or close to triangular) to colinear magnetic structure at H_c, there is incommensurate-commensurate phase transition at $H \approx 3$ T. For details see part 2.3.3.

suggesting that the crossover from the multicritical point takes place slowly, but the specific-heat data and theoretical prediction number 6 both argue against this possibility.

2.3. Heisenberg triangular antiferromagnet with easy-plane type anisotropy

The presence of an anisotropy term in the Hamiltonian with $D > 0$ favours the confinement of spins to the xy plane. The ordered structure in the absence of a field is an equilateral triangle of spins with two chirally-degenerate states as was shown in Fig. 1. For any atom with spin aligned along its local z direction, the local xy degeneracy of the Heisenberg Hamiltonian is broken since a rotation of spins in the plane costs no anisotropy energy while a rotation out of the plane does cost anisotropy energy. This splits a degeneracy in the spin wave excitations, with one acoustic branch having zero energy at magnetic reciprocal lattice points while the other exhibits a gap.

Near the critical point the fluctuations will tend to diverge in the xy plane, but not in the z direction, so that the critical exponents will correspond to the chiral XY, or $Z_2 \times S_1$, model. If D is small there should be a crossover to Heisenberg exponents further away from the critical point. This effect has not been seen to date since only one easy-plane material, $CsMnBr_3$, has had its critical exponents measured extensively, and in this material D is not small compared with J'.

The behaviour of easy-plane triangular antiferromagnets in a small field perpendicular to z involves a competition between the in-plane exchange energy J' and the anisotropy energy D. The J' term is of lowest energy when the moments are aligned in the 120° structure perpendicularly to the field with a canting of the moments towards the field direction, while the anisotropy term favours the 120°

structure aligned in the xy plane. What happens as the field is increased depends on the relative magnitudes of D and J' [134]. At low temperatures, if $D < 3J'$, a field in the xy plane larger than H_s will flip the plane of the spin triangle so that it is perpendicular to the field. This costs anisotropy energy, has virtually no cost in exchange energy, and gains energy from a canting of the spins along the field direction. The spin-flop phase transition will be of first order at

$$g\mu_B H_s = 4S\sqrt{JD} \tag{4}$$

If the anisotropy energy is larger, $D > 3J'$, the ground state above a critical field H_c is one where the spins remain in the plane, but the triangular structure collapses to a colinear structure with two spins in one direction in the plane normal to the field direction and one spin in the opposite direction. This structure costs exchange energy J', has no cost in anisotropy energy, and gains energy by a canting of the spins towards the field direction. The phase transition will be continuous with

$$g\mu_B H_c = 4S\sqrt{3JJ'} \tag{5}$$

It is clear that of these two cases, it is the latter with $D > 3J'$ that corresponds the more closely to the chiral XY model.

Table 6 lists the easy-plane triangular antiferromagnets. All have the ABX_3 structure with strong exchange interactions J and relatively weak in-plane interactions J'. In Table 6 we give the type of antiferromagnet, the space group, the Néel temperature, the critical magnetic field, and the aligned magnetic moment at low temperatures.

In the rest of this section we discuss separately the three cases: small D, large D, and those where the crystal structure is distorted.

2.3.1. The case of small anisotropy $D < 3J'$

There are four materials that are known to be in this category, $CsVCl_3$, $CsVBr_3$, $CsVI_3$, and $RbVCl_3$. The crystal and magnetic structures were established by Zandbergen [45] and by Hauser et al. [32]. Low field susceptibility measurements by Niel et al. [73] on powder samples in the quasi-one-dimensional region ($T \gg T_N$) established the intrachain exchange parameter J for the cesium compounds. Feile et al. [74] measured the spin wave dispersion relations in $CsVCl_3$, $CsVBr_3$, and $CsVI_3$ by neutron inelastic scattering. The measurements were confined to the ($\xi\xi 1$) direction of reciprocal space at low temperatures. The results fitted reasonably with the predictions of linear spin wave theory given by Kadowaki et al. [77] for nearest-neighbour interactions and single-ion anisotropy. The restriction of the data to the plane results in the fitting only giving values for JJ' and JD and a value of J was taken from the paramagnetic magnetization measurements of Niel et al. to determine the values of J' and D given in Table 6. No zero-point-motion correction was made for the reduced moment and one dimensionality so the real values of $|JJ'|$ and $|JD|$ are lower than those quoted. On average, the observed ordered moment on the vanadium atom, as taken from Table 6, is 1.9 μ_B. For $S = 3/2$ with $g = 2$ the maximum moment is 3 μ_B, so the reduction is 63% and the correction to linear spin-wave theory is appreciable.

Little is known experimentally of the phase diagrams or critical properties of these materials. There has been no investigation of the nature of the phase transition in zero field. As pointed out earlier, this is an unresolved area in the theory, with predictions of chiral XY critical exponents, tricritical exponents, and a weak first-order phase transition in the literature. It would be interesting to discover what experiment has to say.

The phase diagram for a field H applied in the xy plane is expected to be as shown in Fig. 5. Phase I is the plane triangular antiferromagnetic structure, phase II is the colinear structure, phase III is the spin-flopped triangular structure, and phase P is paramagnetic. Molecular field calculations by Plumer et al. [131] predict this phase diagram or similar ones differing only by the presence of a narrow region of an extra phase near the first-order transition line. The prediction was

Fig. 5. Magnetic phase diagram of a Heisenberg triangular antiferromagnet with a small easy-plane anisotropy. There is both a tetracritical and a bicritical point.

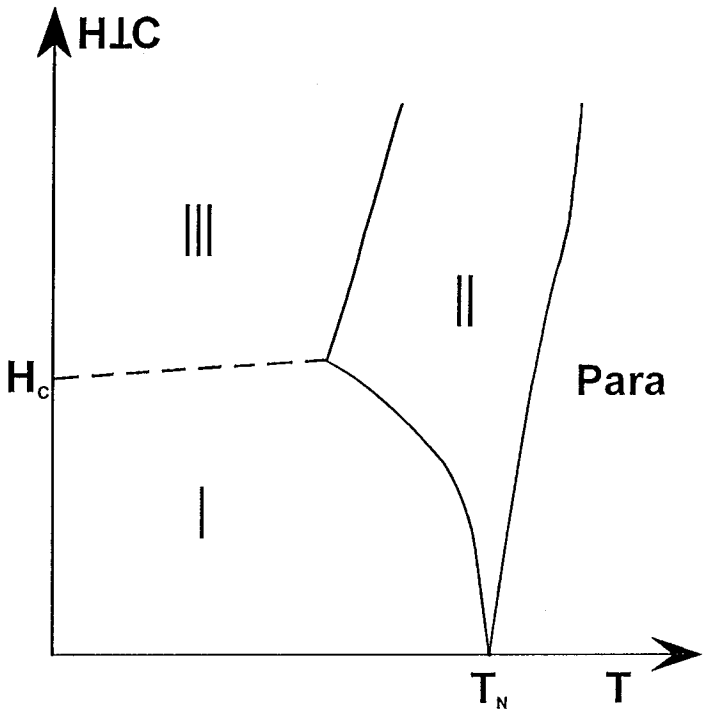

actually for the XXZ Hamiltonian, which is slightly different from our Hamiltonian (1), but the differences are not expected to affect the overall pattern significantly. At $H = 0$ and $T = T_N$ there is a meeting of four phases since at negative H there is a similar phase to phase II with the canting in the opposite direction; thus it is a tetracritical point. The tetracritical nature of the transition shows that it does not belong in the same universality class as the XY model.

Only one critical exponent, ϕ, has been determined in these materials. Near the tetracritical point the two phase boundaries are predicted to behave as [132]

$$H^2 \simeq |T_{Ni}(H^2) - T_N|^{\phi_i} \tag{6}$$

where i has one of two values depending on whether T_{Ni} refers to the phase boundary II, to paramagnetic, or I to II. Actual determination of these exponents is quite sensitive to the value chosen for T_N and to the range of data over which the fit is made [16]. The sum of the two exponents ϕ is much less sensitive to the value of T_N than are the individual values of ϕ.

In $CsVBr_3$, Tanaka et al. [127] have determined the critical exponents ϕ in a field perpendicular to the c direction from susceptibility data. They find $\phi_{P-II} = 0.78(6)$ and $\phi_{I-II} = 0.79(6)$. Scaling and renormalization group theory [2, 7, 123] gives $\phi_{P-II} = \phi_{I-II} = \phi$, with $1 < \phi < \gamma$; for the XY chiral model γ is expected to be only slightly greater than one, probably about 1.1. Thus the experimental values of ϕ are significantly lower than predicted by theory. The discrepancy cannot lie in the sensitivity of the fits to the value of T_N, since the sum of the two individual values of ϕ is just as far from the prediction as is the individual values.

Fig. 6. Magnetic phase diagram of a Heisenberg triangular antiferromagnet with large easy-plane anisotropy. There is a tetracritical point at $T = T_N$ and $H = 0$.

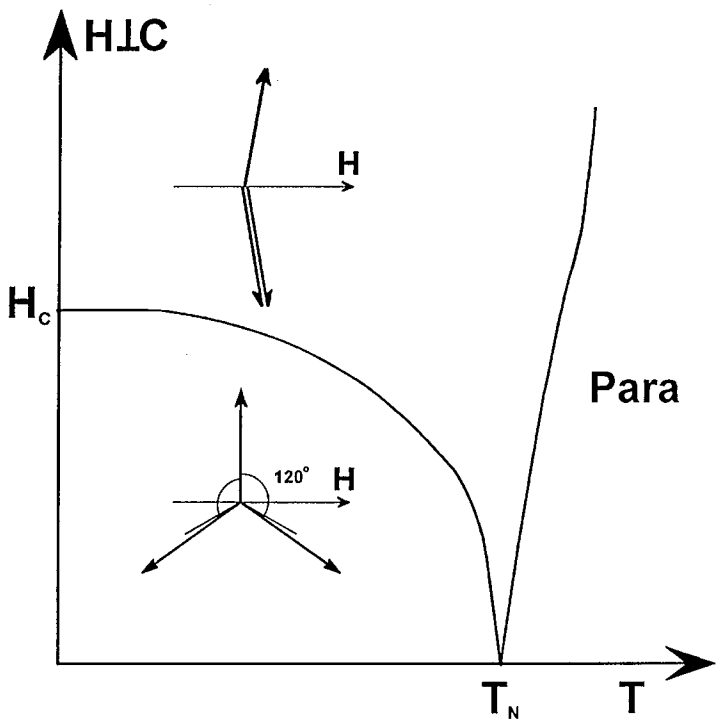

2.3.2. The case of large anisotropy $D > 3J'$

This is the unusual and probably the most interesting case. Although there is only one example of an undistorted triangular easy-plane antiferromagnet that satisfies this condition, $CsMnBr_3$, it has attracted a lot of both theoretical [133–136] and experimental attention through neutron-scattering [11, 12, 43, 67, 68, 137, 138], magnetization [139–141], ESR [142], and specific-heat measurements [126]. As was pointed out in the introduction to this chapter, if $D > 3J'$ the application of a field perpendicular to c no longer produces the spin-flop phase shown in Fig. 5. Instead there is a critical phase transition to an almost colinear structure at a critical field that is given by (5) at $T = 0$. The phase diagram is shown in Fig. 6. At low temperatures and fields the magnetic structure is the 120° stacked triangular structure with the anisotropy confining the moments to within the ab plane. The critical point at $T = T_N$ and $H = 0$ is a tetracritical point just as for the case $D < 3J'$ described in the previous section. In the high-field phase two of the three moments on the triangular lattice become parallel with the third in the antiparallel direction. The moment directions are in the basal plane almost perpendicular to the applied field, but with a small canting towards the field direction proportional to H/J. In this phase there is a softening of one of the exchange branches found by ESR [142].

The nature of the phase diagram was discovered through neutron-scattering measurements of the temperature dependence of the intensity of magnetic Bragg peaks in different fields as shown in Fig. 7 [12]. These results were later confirmed by measurements of the field and temperature dependence of the magnetization as shown in Figs. 8a and 8b. The magnetization process is described satisfactorily in terms of linear spin-wave theory except for two features:

Fig. 7. Temperature dependence of the intensity of magnetic Bragg peaks in $CsMnBr_3$ at $H = 4.2$ T. Successive phase transitions from the paramagnetic phase to the spin-flopped phase and from the spin-flop to the triangular phase occur at 9.0 and 7.15 K, respectively. The inset shows the field dependence of two nuclear Bragg peaks at $T = 7.0$ K. Taken from Gaulin et al. [12]. Reprinted with permission from the publisher and the authors.

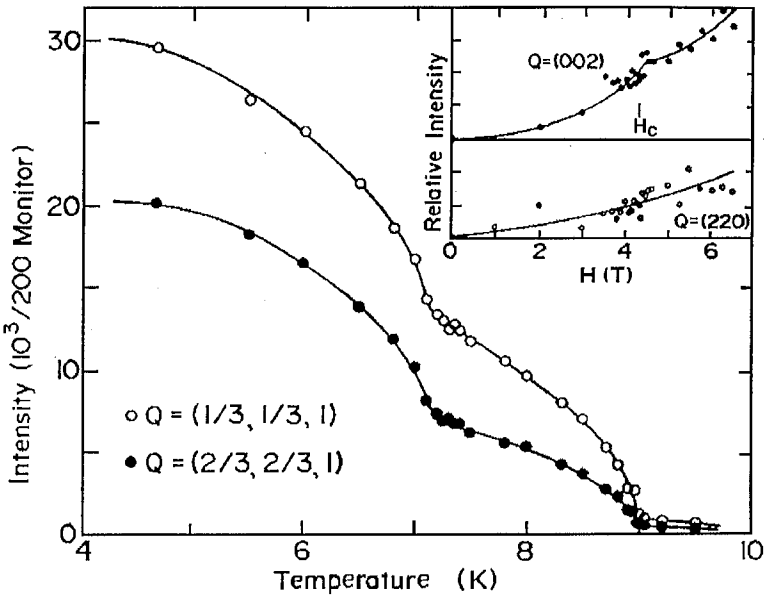

(i) the measured torques are significantly smaller than predicted and

(ii) in high fields, $H > H_c$, there is a considerable anisotropy between the magnetization when the field is applied along and perpendicular to the c axis.

It has been suggested by Abarzhi et al. [141] that quantum fluctuations are responsible for both these effects. This claim has been supported by subsequent work [72, 121] but recently has been disputed by Santini et al. [143], at least for $CsMnBr_3$ and $RbMnBr_3$, where they claimed that the anisotropy is already present at the classical level, provided thermal fluctuations are taken into account. Santini's work is based on a Hamiltonian similar to (1) with the J' term replaced by a dipole–dipole interaction.

A peculiar feature of the phase transition from a triangular to a colinear structure is that it survives even if the field direction deviates significantly from the basal plane. The value of the critical field follows the equation

$$H_c^2(\varphi) = H_c^2 \frac{d-1}{d\cos^2(\varphi) - 1} \tag{7}$$

where $d = D/3J'$ and φ is the angle between the magnetic field and the basal plane, rather than simple field projection on the spin's plane, $H_c(\varphi) = H_c \cos\varphi$ [141].

Kawamura [1, 2] predicted that the easy-plane materials would not follow the XY universality class in their critical properties in zero field because of the extra chiral degeneracy of the order parameter. Instead a new universality class, known as the chiral XY class, would apply. The discovery that the critical point is tetracritical confirms in a simple way that regular XY universality does not apply. The most recent Monte Carlo work, done for the case of ferromagnetic interactions along the c direction, favours a weak first-order phase transition [144–146], with effective critical exponents that are reasonably in agreement with those given by Kawamura for the chiral XY model, less than three errors apart in all cases.

Fig. 8. The field (a) and temperature (b) dependence of the magnetization of $CsMnBr_3$. Taken from Kotyuzhanskii and Nikivorov [140] and from Goto et al. [139]. Reprinted with permission from the publishers and authors.

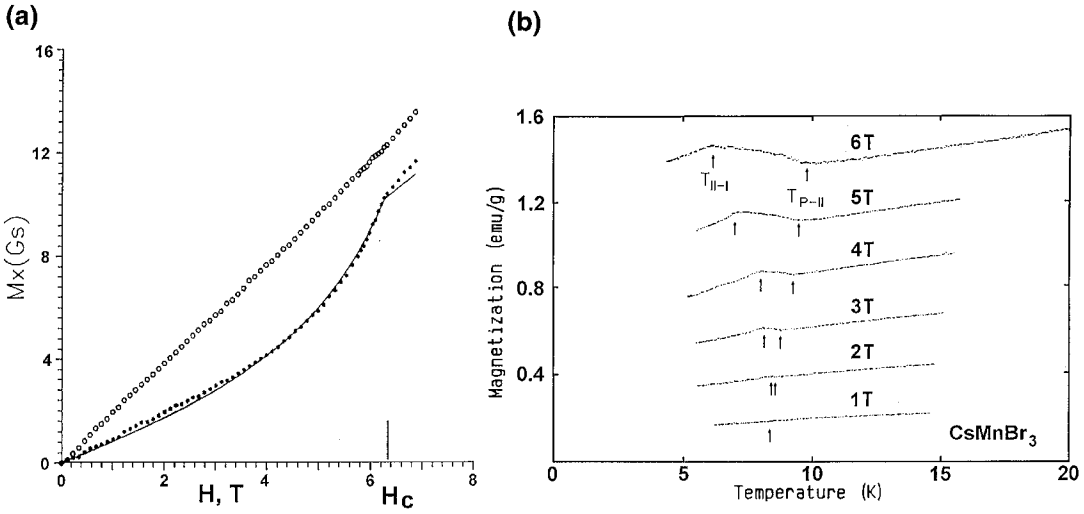

All the known undistorted easy-plane triangular materials are reported experimentally to show critical phase-transitions in zero field in agreement with Kawamura's predictions. Of course it is never possible experimentally to rule out a first-order phase transition if it is sufficiently weak, but critical behaviour is observed to persist at least down to reduced temperatures of 2×10^{-3} [126]. The measured values of the critical indices are listed in Table 7 and compared with the predictions of four possible models: chiral XY, chiral Heisenberg, regular XY, and tricritical in mean-field theory. The exponent $\overline{\phi}$ is the mean of ϕ_{P-II} and ϕ_{I-II}. We use this parameter because Gaulin [16] has shown that while experimental determinations of ϕ_{P-II} and ϕ_{I-II} are highly sensitive to the value of T_N, the mean of the two is much less sensitive, and hence is determined more reliably in experiments. The exponent z is the dynamic critical exponent measured from the temperature dependence of the energy of long-wavelength spin waves [90] near T_N.

The experimental results fit both the chiral XY and the mean-field tricritical models satisfactorily, while they do not fit the other two models. It is not understood why theory and experiment agree so well for the easy-plane case, but less satisfactorily for Heisenberg and easy-axis materials.

2.3.3. Distorted crystal structures

It is not uncommon for the magnetic ABX_3 compounds to experience a crystal distortion. Different types of crystal structure distortions have been found at sufficiently low temperature in $KNiCl_3$, $RbMnBr_3$, $RbVBr_3$, $RbVI_3$, $RbTiI_3$, and $RbFeBr_3$. Generally lattice deformations due to a structural phase transition lead to some modifications of magnetic interactions (the crystal distortions break the symmetry and so change the exchange interaction between neighbouring in-plane magnetic ions) and, consequently, to a partial lifting of frustration on a stacked triangular lattice. Study of such partially frustrated systems is of a fundamental interest, because they do not simply correspond to an intermediate case between unfrustrated and frustrated magnets but show novel physical phenomena absent in the two limiting cases.

Phase transitions to lattices of lower symmetry with decreasing temperature are characterized usually by displacements of chains of magnetic atoms as a whole without deformation so that the intrachain distance between spins remains unchanged. The typical structural transition to the lattice of $P6_3cm$ space group is accompanied by the shift of one from the three adjacent chains upward

Table 7. Experimental values of critical exponents in easy plane materials compared with predictions from various models [16, 126].

Exponent	Experimental value	Chiral XY	Chiral Heisenberg	XY	Mean field tricritical
β	0.22(2) [147] 0.25(1) [148] 0.21(2) [11] 0.24(2) [12] 0.28(2) [149] *	0.25(1)	0.30(2)	0.35	0.25
ν	0.57(3) [150] 0.54(3) [11]	0.54(2)	0.59(2)	0.669	0.50
γ	1.10(5) [150] 1.01(8) [11]	1.13(5)	1.17(7)	1.316	1.00
α	0.39(9) [151] 0.40(5) [152]	0.34(6)	0.24(8)	-0.008	0.50
A^+/A^-	0.19(10) [151] 0.32(20) [152]	0.36(2)	0.54(2)	0.99	—
$\overline{\phi}$	0.98(7) [12] 1.05(5) [139] 0.78(10) [126] 0.79(6) [127] †	$1 < \overline{\phi} < 1.13$	$1 < \overline{\phi} < 1.17$	$1 < \overline{\phi} < 1.32$	
z	1.46(6) [138]	—	—	1.50	—

Experimental values refer to $CsMnBr_3$ except that * and † refer to $RbMnBr_3$ and $CsVBr_3$, respectively.

along the c axis while the two others shift downward keeping the crystal center of mass undisplaced. This primary distortion is shown in Fig. 9.

The crystal unit cell in the basal plane is enlarged to become $\sqrt{3}a \times \sqrt{3}a$ (Fig. 9), preserving the hexagonal symmetry. Because chains are shifted usually only a small distance from the basal plane (~ 0.5 Å in $RbFeBr_3$ [153]), magnetic properties may be considered by placing spins on the same stacked triangular lattice and changing interactions in the Hamiltonian (1) in accordance with a reduced symmetry of the crystal structure. The distortion has little effect on the exchange J along the z direction but in the xy plane the interaction J' is split into two different interactions, $J'_{AB} = J'$ and $J'_{AA} = J'_1$ as shown in Fig. 10a. The $120°$ triangular structure corresponds to $J' = J'_1$ and small departures from this condition give triangular structures with angles not equal to 120°. Mean-field investigations have been carried out to determine the full phase diagram as the ratio of J' to J'_1 is changed [154, 155].

The Hamiltonian of this "centered honeycomb model" (in terms of Zhang et al. [155]) is obtained by the evident replacement of the second term on the right-hand side of (1):

$$J' \sum_{i,j}^{\text{A-A}} \boldsymbol{S}_i \boldsymbol{S}_j + J'_1 \sum_{k,l}^{\text{A-B}} \boldsymbol{S}_k \boldsymbol{S}_l \tag{8}$$

Without field the spin ordering occurs in two steps with additional intermediate colinear phase between T_{N1} and T_{N2} that is either ferromagnetic or partially disordered [156]. The splitting of T_N

Fig. 9. Room temperature crystal structure of $KNiCl_3$, after Visser et al. [158]. The two nickel-chlorine chains within a cell are displaced along the c axis relative to the chains at the cell corners.

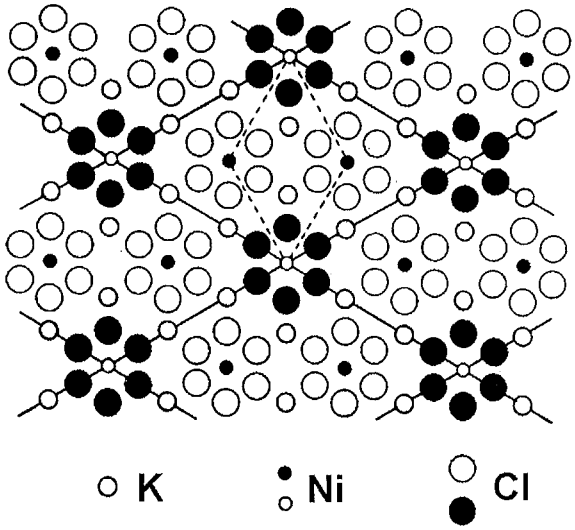

Fig. 10. Magnetic interactions on the distorted triangular lattice: (a) centered honeycomb model; (b) row model.

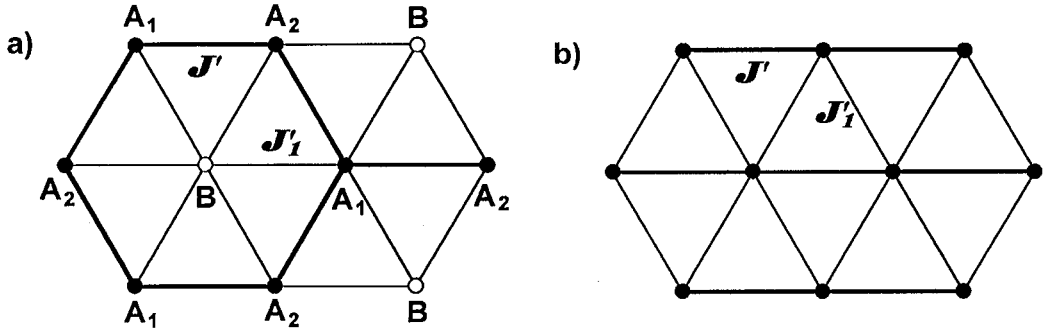

was clearly seen in $RbVBr_3$ [127]. The behaviour of the system in the applied magnetic field depends on the relative strength of exchange constants J' and J'_1. Note, that due to superexchange character of the interchain interaction, it depends in a complicated way on the interatomic distances and bond angles. The critical exponent β at T_{N1} is observed [75] to be 0.32(1), while theory predicts that this phase transition should follow the XY model with β = 0.35.

If $J' < J'_1$, that is coupling between in-plane spins (A_1–A_2 in Fig. 10a) is weaker than coupling between in-plane and out-of-plane spins (A–B), then the presence of the distortion does not change the nature of the phase transition to a colinear phase. The critical field is given in this case by the formula [48]:

$$(g\mu_B H_c)^2 = 48J(2J' - J'_1)S^2 \tag{9}$$

which is very similar to a formula (5) when J' and J'_1 are close to each other.

If $J' > J'_1$, then at low magnetic field, spin of the out-of-plane atom (marked B in Fig. 10a) is aligned parallel to the field. Such a configuration is energetically unfavourable at higher fields,

therefore an additional phase transition occurs at $H^\star < H_c$, when sublattice B starts to deviate from the field direction [157]. Finally, the transition to a colinear phase occurs at

$$(g\mu_B H_c)^2 = 48J(\sqrt{J'^2 + 3J'} - J')S^2 \tag{10}$$

which is again very similar to a H_c in undistorted triangular structure.

The above described theory was developed to explore the magnetic consequences of the crystal phase transition $P6_3/mmc \rightarrow P6_3cm$. Distortions of this type were found in the low-temperature phase of $RbFeBr_3$ [153], at the room temperatures in $KNiCl_3$ [158] and in $RbMnBr_3$ [159], and probably, in $RbVBr_3$ [76]. But, as it will be evident from the discussion given below, in at least two compounds, $RbMnBr_3$ and $KNiCl_3$, further crystal phase transitions just below room temperature play an important role.

In $KNiCl_3$ dielectric anomalies indicating structural phase transitions are found at 274, 285, 561 and 762 K [160]. A single crystal X-ray study on the *low-temperature* structure of $KNiCl_3$ [161] shows clearly the existence of two crystal structure distortions, as originally found by neutron-scattering [130]. One phase (denoted as phase *A*) is hexagonal and does not differ much from the room-temperature structure, the other phase (phase *B*) is orthorhombic. In a phase *A*, the unit cell is rotated through 90° about the c axis from the room-temperature unit cell and enlarged to $\sqrt{3}a$, $\sqrt{3}a$, and c; in a phase *B* the low-temperature unit cell has sizes $2a/\sqrt{3}$, a, and c. The main feature of the phase *B* is a sinusoidal modulation of the ion chains in the basal plane: instead of the room-temperature sequence 0-0-UP-0-0-UP-0-0, where "0" means ion in the basal plane and "UP" means ion slightly shifted above the basal plane along the c axis, at low temperature the sequence is 0-UP-0-DN-0-UP-0-DN-0, where "DN" means the ion is shifted below basal plane. Possible space groups are $Pca2_1$ and $Pbcm$ [161].

As a consequence of the existence of two different crystal modifications, two different magnetic structures have been observed with $T_N = 12.5$ and 8.6 K in phases *A* and *B*, respectively [130]. Magnetization measurements [49] and measurements of ESR [48, 157] showed that in phase *A*, magnetic structure is a distorted triangular with $J' < J'_1$. The magnetic structure of phase *B* we discuss below, for now we just note that in both cases the magnetic structure is commensurate.

In $RbMnBr_3$ the situation with crystal distortion is very similar: the neutron measurements of Heller et al. [71] show a crystal that seems to contain both the *A* and *B* phases, while the measurements of Kato et al. [129] show a crystal where only the *B* phase is present. Moreover, recent X-ray scattering measurements [161] show the total identity of $RnMnBr_3$ and $KNiCl_3$ phase-*B* crystal structures. Such an identity of crystal structure makes it hard to explain the difference in magnetic structure. From a symmetry point of view *B*-phase corresponds to the "row model" of Zhang et al. [155] shown on Fig. 10*b*. Anticipation of this model results in appearance of incommensurate magnetic structure [154,155].

In $RbMnBr_3$, the magnetic structure is indeed incommensurate at low magnetic fields and only if the magnetic field exceeds 3 T it became commensurate [71]. Incommensurate–commensurate phase transition is accompanied by the hysteresis phenomena in magnetization [128], resonance power absorption [162], and magnetic Bragg-peaks intensity [71]. The overall $H - T$ phase diagram, which is much complicated and includes two incommensurate phases, two commensurate phases, and a paramagnetic one, was successfully explained in terms of Landau theory using the row model [163].

In phase *B* of $KNiCl_3$ the magnetic structure is commensurate even in a zero magnetic field [130] and identical to the high-field structure of $RbMnBr_3$. What causes the stabilization of the commensurate spin configuration in $KNiCl_3$ remains unknown.

3. Ising antiferromagnet

The triangular antiferromagnets of type ABX_3 with B a cobalt atom have properties that are like those of Ising antiferromagnets. The cobalt cation lies in an octahedron of X anions with a slight trigonal distortion. The strong crystal field splits the lowest lying ^{4}F configuration so that a $^4T_1$ state

Table 8. Neel temperatures, T_{N1} and T_{N2} K, critical magnetic fields, H_{c1} and H_{c2} T, exchange constants, J and J' GHz, and parameter ϵ for triangular Ising antiferromagnets. Values given for ϵ are for low temperature.

	T_{N1}(K)	T_{N3},T_{N2}(K)	H_{c1}(T)	H_{c2}(T)	J, (GHz)	J', (GHz)	ϵ
$CsCoCl_3$	20.82–NS [33]	5.5,13.5–NS [33]	33.0–M [173]	44.6–M [173]	1557(15)–NS [166]	171–M [27]	0.094(7)–NS [166]
	21.3–NS [167]	9.2(T_{N3})–NS [167]			1541(12)–NS [168]	156–M [170]	0.14(2)–NS [168]
	21–Mö [171]	8.5–Mö [171]			1495(10)–NS [164]	30(2)–NS [164]	0.120(3)–NS [164]
	21.01–NS [172]				1676–M [173]		0.097–M [173]
$RbCoCl_3$	28–Mö [174]		37.8–M [27]	50.2–M [27]	1928–M [27]	186–M [27]	0.091–M [27]
	28–R [175]	11–R [175]			1500–R [175]	45–R [175]	0.1–R [175]
$CsCoBr_3$	28.34(5)–M [41]	12,16–NS [41]	40.6–M [27]	56.6–M [27]	1621(7)–NS [164]	96–NS [164]	0.137(5)–NS [176]
	28.3–Mö [174]	12–Mö [174]			1630–M [27]	211–M [27]	0.106–M [27]
	28.3(1)–NS [177]	12,16–NS [178]					
$RbCoBr_3$	36–NS [37]						

M, Magnetization measurements.

Mö, Mössbauer effect measurements.

NS, Neutron-scattering measurements.

R, Raman scattering measurements.

Fig. 11. Some basal plane ordering of the triangular Ising antiferromagnet with unit cell $\sqrt{3}a$ by $\sqrt{3}a$, as marked by thick lines. Sites marked "+" have $S^z = \frac{1}{2}$, sites marked "-" have $S^z = -\frac{1}{2}$, sites marked "0" have S^z randomly distributed with $< S^z >= 0$, and sites marked $\frac{1}{2}$ have S^z randomly distributed with $< S^z >= \frac{1}{4}$.

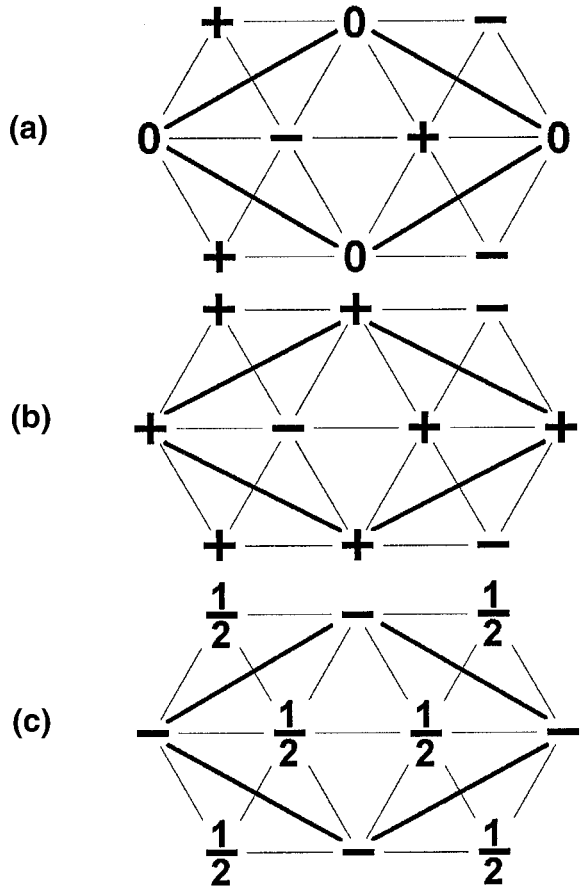

has the lowest energy. This corresponds to a Kramer's doublet, which is effectively an $S = \frac{1}{2}$ state, with the moment lying either parallel or antiparallel to the c axis. There is a mixing between this state and a state of higher energy also with ${}^4T_1$ symmetry and the resultant exchange Hamiltonian at low temperature can be described by the equation [164]

$$\hat{\mathcal{H}} = J \sum_{i,j}^{\text{chains}} [S_i^z S_j^z + \epsilon(S_i^x S_j^x + S_i^y S_j^y)] + J' \sum_{k,l}^{\text{planes}} S_k^z S_l^z - g\mu_{\text{B}} H \sum_i S_i^z \tag{11}$$

with $0 < \epsilon < 1$. In every case ϵ is small, about 0.1, so that the first term in the Hamiltonian, which is of an Ising type, is the dominant term. As in all the ABX_3 triangular systems, the magnitude of the interchain exchange constant J' is small compared with the exchange constant J along the chains. H is an external magnetic field applied along the z direction. A weak single-ion exchange-mixing term can be neglected for the purposes of this article. The parameter ϵ has a weak temperature dependence, decreasing as the temperature is raised [164].

There are four ABX_3 compounds that have the magnetic Hamiltonian given above, $CsCoCl_3$, $RbCoCl_3$, $CsCoBr_3$, and $RbCoBr_3$. There has been extensive work on the first three of these, and

Table 8 lists the experimentally-determined values of the parameters in the Hamiltonian for each compound. We also list values of phase-transition temperatures in zero field, T_N, and of applied fields, H_c, at which there are phase transitions.

Frustration effects are more acute in Ising triangular antiferromagnets than in XY or Heisenberg systems. In the latter cases the frustration can be partially relieved by the formation of a spin triangle as shown in Figs. 1b and 1c, while this is not possible for the Ising antiferromagnet where spins are confined to directions parallel and antiparallel to z. In contrast to the unfrustrated case, Wannier [165] showed that the two-dimensional nearest-neighbour triangular antiferromagnet is disordered at all finite temperatures and has a critical point at $T = 0$. Again the frustration changes the underlying physics.

In the stacked triangular lattice there is no frustration for nearest-neighbour interactions along the stacking direction, whether they are ferromagnetic or antiferromagnetic. This lessening of the overall frustration allows long-range ordering at low temperatures. Figure 11 shows three examples of possible ordering in the basal plane where sites marked " + " have $S^z = \frac{1}{2}$, sites marked " − " have $S^z = -\frac{1}{2}$, sites marked "0" have S^z randomly distributed with $< S^z >= 0$, and sites marked "$\frac{1}{2}$" have S^z randomly distributed with $< S^z >= \frac{1}{2}S = \frac{1}{4}$. In each case the unit cell is $\sqrt{3}a$ by $\sqrt{3}a$, where a is the lattice constant of the triangular lattice. The states shown in Figs. 11a and 11c are not fully ordered, while that shown in Fig. 11b is fully ordered and ferrimagnetic. There is no net ferrimagnetism over the whole crystal in this state however since the strong antiferromagnetic exchange along c ensures that the magnetic moment in a given plane is cancelled by an equal and opposite moment on the next succeeding plane.

The three ordered arrangements shown in Fig. 11 have the same energy, as do many other configurations, so the ground state has a high degree of degeneracy. The unit cell for the three states is the same and their neutron diffraction patterns are similar. In real materials rather small effects may enable the degeneracy to be split in favour of one particular ground state. For instance small ferromagnetic next-nearest-neighbour in-plane interactions will stabilize state (b), while such small antiferromagnetic terms will stabilize state (a).

In the known Ising ABX_3 compounds neutron diffraction in fact indicates the presence of long-range magnetic order. There are sharp peaks of magnetic origin in the neutron-diffraction pattern below a temperature T_{N1}. These peaks are located in reciprocal space at ($\frac{h}{3}$ $\frac{h}{3}$ ℓ), where h is an integer not divisible by three and l is an odd integer. The condition l odd implies antiferromagnetic stacking along the z direction, since the ABX_3 structure has c spacing equal to twice the interplanar spacing. This stacking reflects the strong antiferromagnetic coupling along the c axis. The $\frac{h}{3}$ factors indicate that the unit cell in the xy plane is $\sqrt{3}a$ by $\sqrt{3}a$. This is not an unexpected result in view of the discussion earlier regarding Fig. 11. In Figs. 12 and 13, taken from Yelon et al. [41] and Mekata and Adachi [33], respectively, the temperature dependence of some observed neutron-scattering Bragg peaks is shown for $CsCoBr_3$ and for $CsCoCl_3$. These measurements show that the temperature dependence of the ordering is not simple. Some rearrangement of the ordered structure at temperatures below T_{N1} is taking place, without changing the unit cell or broadening the magnetic Bragg peaks. Similar results have also been reported by Farkas et al. [178] in $CsCoBr_3$ and by Yoshizawa and Hirakawa [167] in $CsCoCl_3$. Detailed analysis has shown that the high-temperature ordered structure in both materials is similar to that shown in Fig. 11a. Neutron critical scattering has been observed around ($\frac{1}{3}\frac{1}{3}1$) at temperatures close to T_{N1} in $CsCoBr_3$ [177].

As is shown in the figures, a feature of the low-temperature neutron-scattering from $CsCoBr_3$ and $CsCoCl_3$ is the presence of a (111) magnetic Bragg peak. This peak has the scattering from the three magnetic sites in each basal plane in phase, while there is a phase reversal between successive planes. Thus its intensity reflects the net magnetic moment in each plane. At temperatures below T_{N3} (12 K in $CsCoBr_3$ and 5.5 K in $CsCoCl_3$) each plane is ordered ferrimagnetically and the ordering corresponds to that shown in Fig. 11b. Neutron critical scattering has been observed around (111) at

Fig. 12. Temperature dependence of some of the strong magnetic reflections in $CsCoBr_3$. There are two critical phase transitions at $T_{N1} = 28$ K and at $T_{N2} = 12$ K. The figure is taken from ref. 41 and reprinted with permission of the publisher.

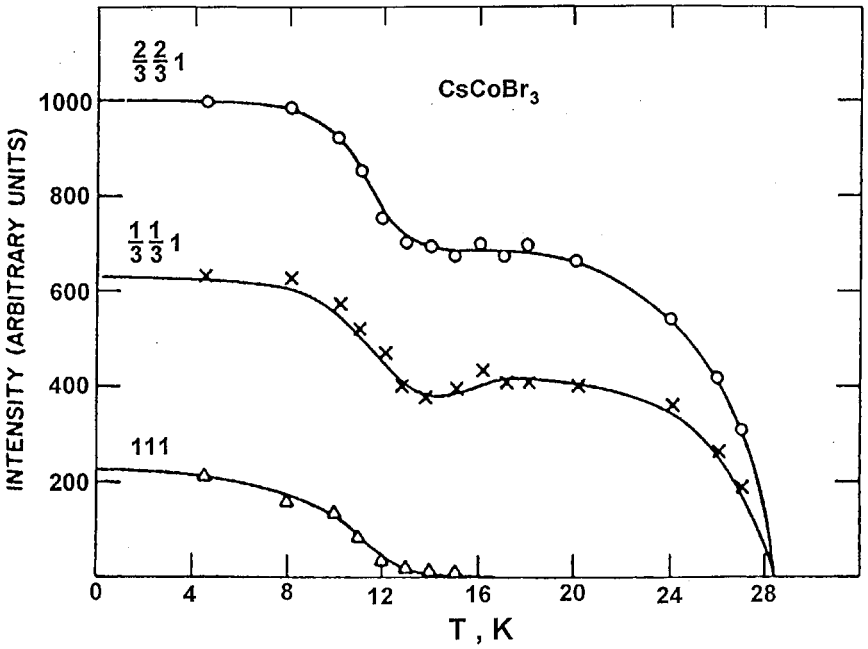

temperature close to T_{N3} in $CsCoCl_3$ [179]. The absence of magnetic intensity in the (001) Bragg peak indicates that the moments are ordered in the c direction. At temperatures between T_{N3} and $T_{N2} = 13.5$ K in $CsCoCl_3$ there is clearly some structural rearrangement taking place. This is less evident in $CsCoBr_3$, but the data do seem to indicate some small reduction of the magnetic intensities as the temperature is lowered from $T_{N2} = 16$ K [41, 178] to T_{N3}. Exactly what is happening in the intermediate region between T_{N2} and T_{N3} has not been established by the experimental work to date. In assigning values to T_{N2} and T_{N3} in $CsCoBr_3$, we have reinterpreted the data of Yelon et al. to be on a consistent basis with the assignments by other authors [33, 167, 178].

Two experimental features should be mentioned here. First in $CsCoBr_3$, Yelon et al. [41] indicate that there is also a small component of ordered moment in the xy plane, but this has not been reported in the work on $RbCoBr_3$ or $CsCoCl_3$. If confirmed, such ordering would arise from the term involving the parameter ϵ in (11) and indicates departure from the Ising form. Second, a perhaps surprising experimental result is that, although the specific-heat has a clear anomaly at T_{N1}, there is no feature corresponding to the transitions at T_{N2} and T_{N3} [41, 180].

Theory has concentrated on the solution to the true Ising system on the basis of the Hamiltonian given in (11) with $\epsilon = 0$. There has also been work with next-nearest-neighbour interactions in the basal plane included, so as to reduce the ground state degeneracy. The ground state in the Landau–Ginzburg–Wilson (LGW) model is shown as (c) in Fig. 11 [181]. There is a transition at temperature T_{N2} to a second ordered state corresponding to Fig. 11a where one sublattice has a zero mean value of S^z. Plumer et al. [182] show that, if the LGW treatment is expanded to higher order in the spin density, the phase transition can split into two transitions at T_{N2} and T_{N3}, although the splitting, $(T_{N2} - T_{N3})/T_{N3}$ is small, of order 1%. The specific-heat effects are of opposite sign and tend to cancel, agreeing with the experimental findings.

Fig. 13. Temperature dependence of peak intensity of typical magnetic reflections of $CsCoCl_3$. Continuous curves are calculated values. The figure is taken from ref. 33 and reprinted with permission from the publisher and the authors.

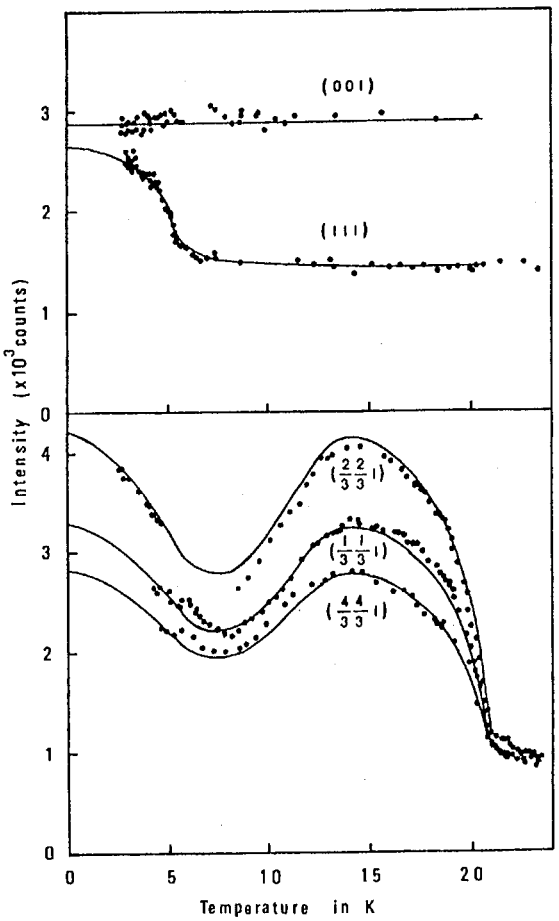

As discussed earlier, [33, 37, 183] experiments at low temperatures indicate the presence of an ordered state that corresponds to Fig. 11b in contradiction to the predictions of the LGW model. Kurata and Kawamura [184] have recently shown that an extension of mean-field theory to include correlation effects in the xy plane can give the observed ferrimagnetic ground state.

Even after this difficulty is taken care of, however, the LGW treatment still has shortcomings as it does not give the correct low-temperature state, which Coppersmith [185] has shown involves some disorder on every site. The various experiments refered to above report similar values of the ordered moment at low temperature with a mean of 3.2(2) $\mu_{\rm B}$. There is no appreciable difference between the predicted maximum ordered moment of $g_{\|}\mu_{\rm B}S$ [27] and the measured moment, so the amount of the disorder is not large. However, the recent NMR work of Kohmoto et al. [186] shows direct evidence of the presence of disorder at low temperatures as predicted.

Another approach to the solution of the frustrated Ising model is to use Monte Carlo methods. Matsubara et al. [187–189] have shown that this gives the ferrimagnetic phase at low temperatures and two other ordered phases at higher temperatures, in good agreement with experiment. The high-temperature ordered phase, between T_{N1} and T_{N2}, is a randomly modulated phase (RMP). Although the long-range order persists on a $\sqrt{3}a$ by $\sqrt{3}a$ cell, there is a random modulation of S^z on all three

Table 9. Comparision of different determinations of the critical indices for the phase transition from an ordered state to a paramagnetic state in Ising antiferromagnets.

	Method	α	β	γ	ν
3D XY model [90]	Consensus	$-0.01(2)$	0.345(12)	1.316(9)	0.669(7)
Matsubara [189]	Monte Carlo		0.32(2)		
Bunker et al. [191]	Monte Carlo	$-0.05(3)$	0.311(4)	1.43(3)	0.685(3)
Plumer, Mailhot [192]	Monte Carlo	0.012(30)	0.341(4)	1.31(3)	0.662(9)
Yelon et al. [41]	Neutron		0.31(2)		
Mekata, Adachi [33]	Neutron		0.34(1)		
Mekata et al. [172]	Neutron		0.352		
Farkas et al. [178]	Neutron		0.22(2)		
Wang et al. [180]	Spec. heat	$-0.025(4)$			

sites. The order parameter is the magnetic structure factor,

$$f(\boldsymbol{Q}) = \sum_j S_j^z \, \mathrm{e}^{i\boldsymbol{R}_j \cdot \boldsymbol{Q}} \tag{12}$$

with $\boldsymbol{Q} = (\frac{1}{3}\frac{1}{3}1)$. The low-temperature structure, with $T < T_{N3}$, also has $f(\boldsymbol{Q})$ as the order parameter, but with $\boldsymbol{Q} = (001)$. The transitions at T_{N1} and T_{N3} are critical phase transitions, but the nature of the transition at T_{N2} is not clear. Between T_{N2} and T_{N3} the structure is complex with the characteristics of the RMP phase present, but with an anomalous temperature dependence of the order parameter $f(\frac{1}{3}\frac{1}{3}1)$. Neutron scattering is a direct technique for characterizing the phase transitions at T_{N1} and at T_{N3} because it can measure the scattering around $(\frac{1}{3}\frac{1}{3}1)$ and (001) directly. It is an unanswered question whether there is a true phase transition at T_{N2}, though there clearly is a region just above T_{N3} where the magnetic order has unusual temperature dependence. There is qualitative agreement between the neutron-scattering data and the Monte Carlo work both with regard to the temperature dependence of the magnetic structure factors and to the ratio of T_{N1} to T_{N2} and to T_{N3}. Further the Monte Carlo computations show no specific-heat anomaly at T_{N2} or at T_{N3}, in agreement with experiment.

The nature of the phase transition at T_{N1} has received much attention, both theoretically and experimentally. Berker et al. [181] used renormalization group arguments to predict that the transition is in the same universality class as the order–disorder phase transition in the three-dimensional XY model.

Early Monte Carlo work on the phase transition was done by Matsubara and Inawashiro [189] and by Hienonen and Petschek [190] but the most accurate analysis comes from the work of Bunker et al. [191] and Plumer and Mailhot [192]. There is controversy concerning the accuracy of some of these results, with Plumer and Mailhot's work showing satisfactory agreement with the three-dimensional XY model while that of Bunker et al. shows significant discrepancies. Table 9 lists the values obtained by these authors and a comparison with the XY model and with experiment. Apart from those of Farkas et al., the experimental results for β cover the same range as the theoretical values, with a weak bias towards the higher values. The experimental value for α claims higher accuracy than any of the theoretical values but again no definitive conclusions can be made. The Monte Carlo simulations of Plumer et al. [193] indicate that the critical region at T_{N1} is smaller than usual due to the proximity of another ordered phase that is would be stabilized by next-nearest-neighbour interactions of order 10% of J'. The recent neutron-scattering work of Rogge [177] on $CsCoBr_3$ shows results incompatible with a normal critical phase transition, in that the critical fluctuations cannot be described in terms of a model with a single length scale. This whole situation is unclear and more work is needed to

Fig. 14. Magnetization process of $CsCoCl_3$ along the c axis at several temperatures, after Amaya et al. [173]. At low temperature there are phase transitions at $H_{c1} = 33$ T and at $H_{c2} = 45$ T. Reprinted with permission of the publisher and the authors.

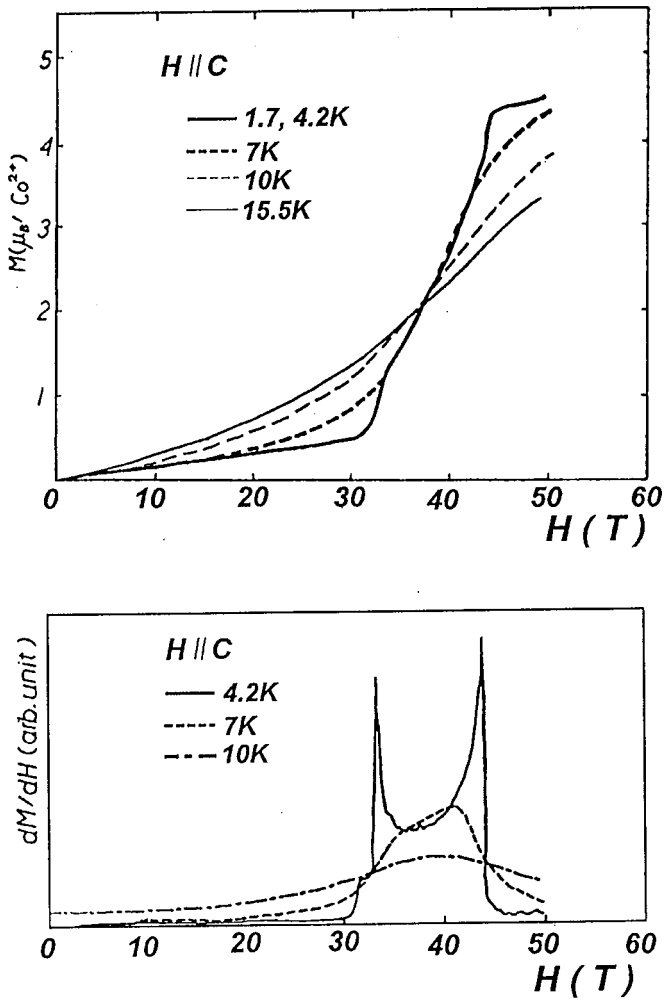

resolve it.

Because of the Ising nature of the Hamiltonian and the quasi-one-dimensional nature of the magnetic interactions, the excitations in these compounds are predominantly of the soliton type. Solitons have been observed in both $CsCoCl_3$ [164,179] and $CsCoBr_3$ [164,176,194] and the results used to determine the parameters J and ϵ in the Hamiltonian (equation (11)).

Boucher et al. [179] show that soliton excitations are present at temperatures down to T_{N3}. The neutron-scattering data near the phase transition at T_{N1} have been interpreted in terms of a soliton condensation on to one sublattice to give a magnetic structure of the type shown in Fig. 11*b* with the solitons on the chains corresponding to the sites with zero mean moment [16,195]. This result is not in accord with the idea of a randomly modulated phase [189] from Monte Carlo simulations. Since all the Monte Carlo work has been carried out for much-less-one-dimensional Hamiltonians (smaller values of J/J') than is found in actual ABX_3 compounds, and since the soliton ideas are products of

the one dimensionality, the soliton measurements [179, 195] raise questions about whether the Monte Carlo simulations map on to the real materials, particularly as the excitations are fundamentally different.

We conclude this section with a discussion of the effect of a magnetic field on triangular Ising antiferromagnets. Consider first a one-dimensional Ising antiferromagnet with nearest-neighbour interactions. The Hamiltonian is

$$\hat{\mathcal{H}} = J\sum_{i,j} S_i^z S_j^z - g\mu_{\mathrm{B}} H \sum_i S_i^z \tag{13}$$

Yang and Yang [196] give an exact solution of this Hamiltonian, but here we just treat the basic ideas. At low temperature and $H = 0$ the system will form antiferromagnetic chains with a few solitons breaking the long-range order. The field will have only small effects until it reaches a critical value H_{c} where it can break antiferromagnetic bonds without cost in energy.

$$g_{\parallel}\mu_{\mathrm{B}} H_{\mathrm{c}} = 2|J| \tag{14}$$

At field H_{c} there should be a phase transition from antiferromagnetism to ferromagnetism. This transition is observed in the ABX_3 Ising compounds, though the field H_{c} is large (~ 40 T) because the exchange J along the chains is large.

In the ferrimagnetic-plane low-temperature structure (Fig. 11*b*) the small interchain exchange J' results in there being two critical fields, $H_{\mathrm{c}1}$ and $H_{\mathrm{c}2}$. At field $H_{\mathrm{c}1} = H_{\mathrm{c}}$ one of the chains marked "+" in the figure becomes ferromagnetic without cost in interchain exchange energy. The magnetisation per cobalt atom is $g_{\parallel}\mu_{\mathrm{B}} S/6$. Then at a higher field $H_{\mathrm{c}2}$ the other two chains become ferromagnetic, with

$$H_{c2} = H_{c1} + \frac{6|J'|}{(g_{\parallel}\mu_B)} \tag{15}$$

and the magnetization per cobalt atom is $\mathrm{g}_{\parallel}\mu_{\mathrm{B}} S/2$.

Figure 14 shows the magnetization plotted against the applied field as observed in $CsCoCl_3$ by Amaya et al. [173]. The two steps in the magnetization are not seen, but instead there is a rounding out between $H_{\mathrm{c}1}$ and $H_{\mathrm{c}2}$ which is not expected from the simple arguments that we have given. As the figure shows, this rounding becomes more pronounced at higher temperatures in the ordered phase. The critical fields, $H_{\mathrm{c}1}$ and $H_{\mathrm{c}2}$ are usually identified with the two maxima in $\mathrm{d}M/\mathrm{d}H$, and it is these values that are shown in Table 8.

Table 8 shows that the values of J derived from $H_{\mathrm{c}1}$ agree reasonably with those found by other experimental techniques, but the values of J' derived from $H_{\mathrm{c}2} - H_{\mathrm{c}1}$ seem to be significantly higher than values from other experimental techniques. They give J/J' of order 10, which is surprisingly small. Even the larger ratios found from neutron and Raman scattering are appreciably smaller than is found in Heisenberg ABX_3 compounds (Table 2), indicating that the cobalt compounds are less one dimensional in magnetic properties.

4. Singlet-ground-state magnets

This chapter is devoted to the description of the magnetic properties of four compounds from the $AFeX_3$ family: $CsFeCl_3$, $CsFeBr_3$, $RbFeCl_3$, and $RbFeBr_3$. At room temperature they all have the same crystal structure with space group $P6_3/mmc$ and, as usual for all ABX_3 hexagonal compounds, at low temperature they exhibit quasi-one-dimensional magnetic behaviour. A characteristic property of these four crystals is the large value of the magnetic anisotropy in comparison with the exchange interaction. In some cases this prevents the advent of long-range magnetic ordering (LRO) even

Fig. 15. Energy levels of Fe^{2+} in the $AFeX_3$ family.

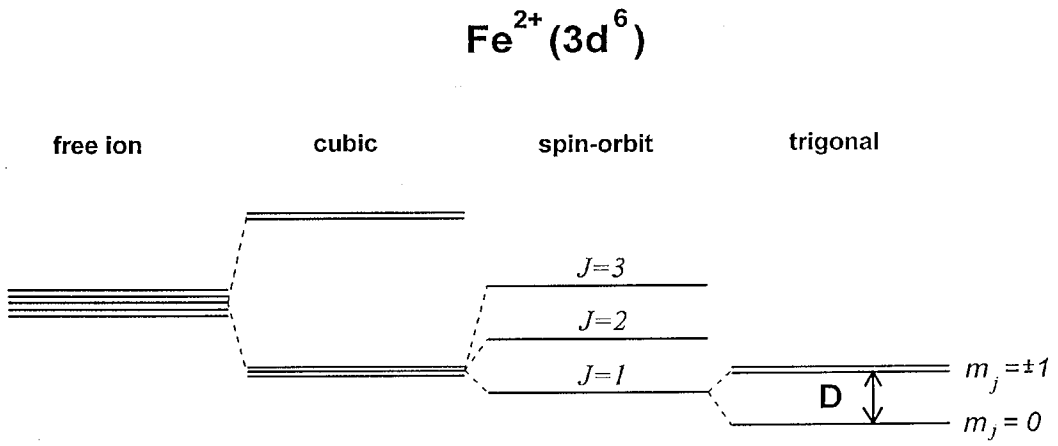

at zero temperature. There are other compounds (ND_4FeBr_3, ND_4FeCl_3, $TlFeBr_3$, $TlFeCl_3$, and $CsFeI_3$) that probably may be described as singlet-ground-state magnets [197, 198], but they have been investigated less thoroughly and a comprehensive understanding of their physical properties has not yet been developed.

A free Fe^{2+} ion in the $AFeX_3$ family has a ${}^5D$ ground state. A cubic crystal field splits this into an upper orbital doublet and a lower orbital triplet with an energy difference of order 1000 cm^{-1}. Spin-orbit coupling, λ', causes a further splitting of the triplet according to the effective total angular momentums $\mathcal{J} = 1$, 2, and 3. The lowest state with $\mathcal{J} = 1$ is split still further by a trigonal component of the crystal field, Δ', to produce a singlet ground state ($m_{\mathcal{J}} = 0$) and an excited doublet ($m_{\mathcal{J}} = \pm 1$) as shown in Fig. 15. The Hamiltonian representing these splittings of the triplet state may be written as

Since the energy separation between the ground state and the second excited state is of order of 100 cm^{-1} [200], at low temperature only the first excited doublet is appreciably populated and the following effective spin Hamiltonian can be used to describe the magnetic properties of $AFeX_3$ compounds:

$$\hat{\mathcal{H}} = \sum_{i,j}^{\text{chains}} [J_\perp (S_i^x S_j^x + S_i^y S_j^y) + J_\parallel S_i^z S_j^z] + \sum_{k,l}^{\text{planes}} [J'_\perp (S_k^x S_l^x + S_k^y S_l^y) + J'_\parallel S_k^z S_l^z]$$
$$+ D \sum_i (S_i^z)^2 - \mu_B \sum_i [g_\perp (S_i^x H_x + S_i^y H_y) + g_\parallel S_i^z H_z] \qquad (16)$$

where $S = 1$ is fictitious spin and D, the value of which is positive, equals the energy gap between the $m_{\mathcal{J}} = 0$ and $m_{\mathcal{J}} = \pm 1$ states. However, some authors prefer to use the Heisenberg Hamiltonian (1) to describe magnetic properties of the linear chains antiferromagneticaly coupled Fe^{2+} ions in $CsFeBr_3$ and $RbFeBr_3$.

$$\hat{\mathcal{H}} = \Delta'(L_{iz}'^2 - 2/3) + \lambda' \boldsymbol{L}'_i \boldsymbol{S}'_i \qquad (17)$$

Fig. 16. Energy level structure of the effective single-ion Hamiltonian [16] for $H \parallel c$ (top) and $H \perp c$ (bottom).

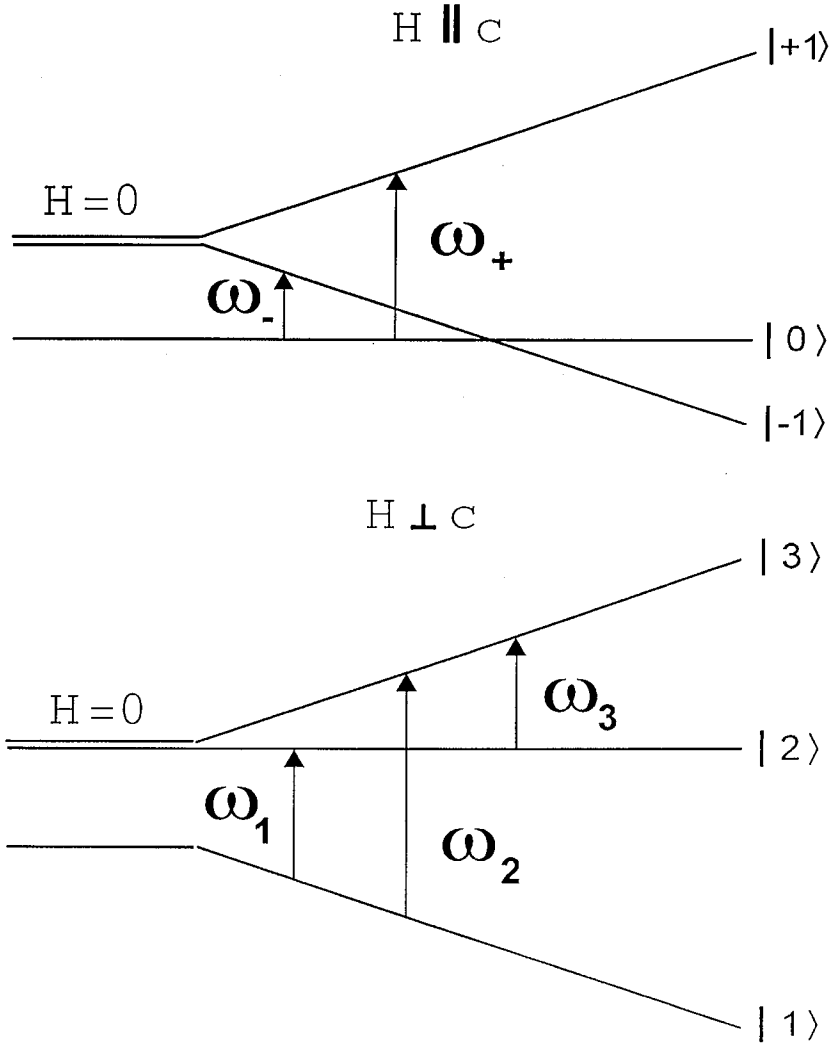

As $T \to 0$ in the absence of an external magnetic field there are two regimes separated by a phase transition.

1. For $D < 8\,|J| + 12\,|J'|$ the system has a magnetic ground state with an easy-plane type of anisotropy. This is the case for $RbFeCl_3$ and $RbFeBr_3$.

2. For $D > 8\,|J| + 12\,|J'|$ the system has a singlet ground state and consequently does not order magnetically even at $T = 0$. This is the case for $CsFeCl_3$ and $CsFeBr_3$.

The equality $D = 8\,|J| + 12\,|J'|$ was derived as a condition at which the lowest excitation energy gap at the magnetic zone center becomes zero [29].

The application of an external magnetic field along c axis on the SGS materials leads to a phase transition to an ordered state. This happens at a field H_c, when one of the excited doublet levels crosses the ground-state singlet level, as it shown on Fig. 16. In $CsFeCl_3$ a commensurate 120°

ordered structure appears after intermediate transitions through two incommensurate structures, while in $CsFeBr_3$ the phase transition leads directly to commensurate order. If the external magnetic field is applied perpendicular to the c axis, the singlet level remains below the excited levels at all fields so that no LRO is expected.

Before going to the detailed description of each compound we summarize some characteristics of each material in Table 10. An attempt to analyze the correlation between the structural and magnetic parameters of the $AFeX_3$ family of compounds is made by Visser and Harrison in ref. 199.

4.1. The case of antiferromagnetic intrachain coupling

4.1.1. $CsFeBr_3$

In $CsFeBr_3$ and $RbFeBr_3$ all exchange interactions are antiferromagnetic. Except for an early susceptibility measurement by Takeda et al. [217], the works on $CsFeBr_3$ are devoted to the investigation of the magnetic excitations. The excitation spectrum was studied both theoretically [218–221] and experimentally by means of inelastic neutron-scattering in a zero field [42, 210] and in an external magnetic field [209, 211, 222].

The lowest frequency excitation mode softens with decreasing temperature but stabilizes at 0.11 THz below 2.5 K down to 80 mK [209]. This fact indicates that $CsFeBr_3$ remains a SGS system for $T \to 0$ in zero field. At 1.6 K in an external magnetic field of 4.1 T applied along c axis a well-defined Bragg peak appears at (2/3 2/3 1) indicating a phase transition to the long-range commensurate 120° structure [222]. But the correlation lengths do not diverge at that field. Instead, they exhibit a flat maximum over about 0.3 T around 4.1 T and decrease again at higher field [209]. The nature of this phenomena is not yet understood.

4.1.2. $RbFeBr_3$

This compound can be considered as an intermediate case between the SGS antiferromagnet and the Heisenberg antiferromagnet with easy-plane anisotropy; the exchange interaction is strong enough to produce three-dimensional order at temperatures below 5.5 K [153]. At a temperature of 108 K $RbFeBr_3$ undergoes a structural phase transition to a distorted phase with space group $P6_3/mmc$ [216], which results in the appearance of two kinds of nearest-neigbours exchange in the basal plane (J' and J'_1). This produces a distortion of a spin triangles with the angle between nearest spins not exactly 120°. The spin frustration is partially released (see Sect. 2.3.3 for details). The low temperature crystal phase is found to be ferroelectric [223].

The specific-heat measurements revealed two successive magnetic phase transitions at $T_{N1} = 5.61$ K and $T_{N2} = 2.00$ K [215]. This may be caused by the splitting between J' and J'_1, but in fact the J'/J'_1 ratio remains experimentally unknown: the inequivalency of the Fe^{2+} sites is not sufficiently large to be distinguished by Mössbauer spectroscopy [214]; the resolution of the inelastic neutron-scattering experiments [38] was not good enough to see the influence of the splitting on the dispersion of magnetic excitations. The energies and intensities of the excitations can be described well using the dynamical correlated effective-field approximation neglecting the splitting between J' and J'_1.

4.2. The case of ferromagnetic intrachain coupling

4.2.1. $CsFeCl_3$

In $CsFeCl_3$ the exchange interaction between Fe^{2+} ions is ferromagnetic along the c axis, while the interchain exchange is weakly antiferromagnetic [201]. The results of inelastic neutron scattering [29] show that at $T = 5$ K the lowest excitation energy at the magnetic zone center has a peak about 190 GHz confirming the absence of long-range magnetic order. From the dispersion relations the parameters in the effective spin Hamiltonian (16) may be obtained, but the results depend strongly

Table 10. Characteristics of the SGS triangular antiferromagnets.

	Space group at low T	T_N(K)	Parameters of the magnetic interaction (GHz)
$CsFeCl_3$	$P6_3/mmc$	LRO not found down to 0.8 K (C) [203], 80 mK [204]	$D = 308, J = -148, J' = 40$ (INS, heuristic formula) [201, 202] $D = 523, J_\perp = -54.5, J'_\perp = 2.88$ (INS, exciton model) [29] $D = 387, J_\parallel = -75, J_\perp = -150$ (Mö, pair model) [205] $D = 522, J = -62.9, J' = 4.2$ (INS, RPA) [206] $D = 416, J_\parallel = -73, J_\perp = -110$ (NMR, spin-band model) [207] $D = 420, J = -78, J' = 4.2$ (INS, DCEFA) [208]
$CsFeBr_3$	$P6_3/mmc$	LRO not found down to 80 mK (NS) [209]	$D = 620, J = 66, J' = 6.7$ (INS, RPA) [42] $D = 620, J = 66, J' = 6.2$ (INS, RPA) [210] $D = 640, J = 64, J' = 8$ (INS) [211]
$RbFeCl_3$	$P6_3/mmc$	2.55 [212] 2.45 (Mö) [205]	$D = 360, J_\parallel = -150, J_\perp = -330$ (Mö, pair model) [205] $D = 408, J_\parallel = -110, J_\perp = -120, J'_\perp = 16$ (INS, 3 sublat. model) [29] $D = 580, J_\perp = -65, J'_\perp = 6.0$ (INS, exciton model) [29] $D = 498, J_\parallel = -30, J_\perp = -66$ (INS, DCEFA) [213]
$RbFeBr_3$	$P6_3cm$	5.5 (NS) [153] 5.61 and 2.00 (C) [215]	$D = 250 - 270, J = 52, J' = 2$ (Mö, CEFA) [214] $D = 1580, J = 26, J' = 5.8$ (INS, SW-theory) [216] $D = 1580, J = 26, J' = 5.8$ (INS, SW-theory) [216]

LRO, long-range order.

INS, inelastic neutron-scattering measurements.

C, specific-heat measurements.

Mö, Mössbauer effect measurements.

NMR, nuclear magnetic resonance.

RPA, random phase approximation.

DCEFA, dynamical correlated-effective-field approximation.

upon the theoretical model used to analyze the experimental data. An exciton model, correlated effective field analysis [29], self-consistent random-phase approximation [220], and dynamical correlated effective-field approximation [208] give substantially different values for the exchange interaction and the magnetic anisotropy. The parameters of the spin Hamiltonian can be estimated also from measurements of the Mössbauer effect [205] and of the nuclear spin-lattice relaxation time [207] (see Table 10 for details).

Further inelastic neutron-scattering investigation of the dispersion curves in the $CsFeCl_3$ [206] has shown that the minimum of the dispersion curve does not occur at the K-point but is shifted slightly away. This effect can be explained by the inclusion of dipolar forces [224, 225].

The transition to a magnetically ordered phase in an external magnetic field was detected by magnetization [207, 226, 227], specific-heat [226], Mössbauer [228], and nuclear spin-lattice relaxation [207] measurements. At $H_c = 7.5$ T the ordered state was observed at $T < 2.6$ K. Because measurements are necessarily made at nonzero temperature, LRO appears over a wide region of magnetic field around H_c. For example at $T = 1.3$ K magnetic susceptibility shows two anomalies at 3.8 and 4.6 T when LRO appears, and the same two anomalies at 11.2 and 11.6 T when LRO disappears in an increasing field. The step structure in the $\mathrm{d}\mathbf{M}/\mathrm{d}\boldsymbol{H}$ curve observed at 3.8 and 4.6 T is caused by successive phase transitions from the nonmagnetic phase to a thermally frustrated incommensurate phase and then to a commensurate three-sublattice antiferromagnetic phase [227]. An incommensurate magnetic phase (double-modulated and single-modulated) was found between the nonmagnetic phase at low field and the commensurate phase at higher field by means of elastic neutron-scattering [202]. At $T = 0.7$ K the magnetic phase transitions take place at $H_1 = 3.85$ T, $H_2 = 3.92$ T, and $H_3 = 4.5$ T. A possible explanation of the nature of the incommensurate phases has been given in a framework of the correlation theory [220, 229].

An additional magnetic phase transition at 33 T was observed in a magnetization measurements [227]. The high field magnetization cannot be explained within the framework of the fictitious $S = 1$ spin states. Since the magnitude of themagnetization at 33 T is large, the anomalous increase in $\boldsymbol{M}$ is attributed to the upper excited $\mathcal{J} = 2$ spin state [227].

All five possible transitions for $H \parallel c$ and $H \perp c$ between the ground state and the excited doublet (see Fig. 16) have been observed in submillimetre wave ESR-measurements [230], while at higher frequencies only two absorption lines were observed using far infrared Fourier spectroscopy [231]. One of the absorptions seems to come from the excitation between the ground state and the second excited doublet. The mechanism of the second absorption is still unclear.

4.2.2. $RbFeCl_3$

Unlike $CsFeCl_3$, the isomorphous compound $RbFeCl_3$ reveals three-dimensional long-range magnetic order below $T_{N1} = 2.55$ K [212]. The signs of the exchange interactions are the same as in $CsFeCl_3$—ferromagnetic along the c axis and antiferromagnetic in the plane. An inelastic neutron-scattering study [29, 169] showed clear softening of the magnetic excitations in a small region around the zone center when $T \to T_{N1}$. The influence of the softening on the nuclear spin-relaxation time T_1 of ^{87}Rb was observed in an NMR experiment [232]. According to an elastic neutron-scattering study [233] at zero magnetic field, $RbFeCl_3$ undergoes three transitions at $T_{N1} = 2.5$ K, $T_{N2} = 2.35$ K, and $T_{N3} = 1.95$ K. Two different incommensurate structures have been found at $T_{N3} < T < T_{N2}$ and $T_{N2} < T < T_{N1}$, while at $T < T_{N3}$ the 120° in-plane triangular structure is observed [29, 212, 233]. Very similar values for the phase-transition temperatures have been found from specific-heat and susceptibility measurements [226]. The existence of thermal hysteresis at T_{N3} indicates that the incommensurate–commensurate transition is first order. From this study and susceptibility measurements [234] a phase diagram in (H, T) coordinates may be derived as shown in Fig. 17. There are two main features (a) the 120°-structure and paramagnetic phase are always separated by one or two incommensurate phases; (b) application of a magnetic field parallel to the c axis

Fig. 17. Magnetic phase diagram of the $RbFeCl_3$ for $H \perp c$, after Wada et al. [234]. Open and closed circles correspond to the anomalies observed in the specific-heat and susceptibility measurements, respectively. Reprinted with permission from the publisher and the authors.

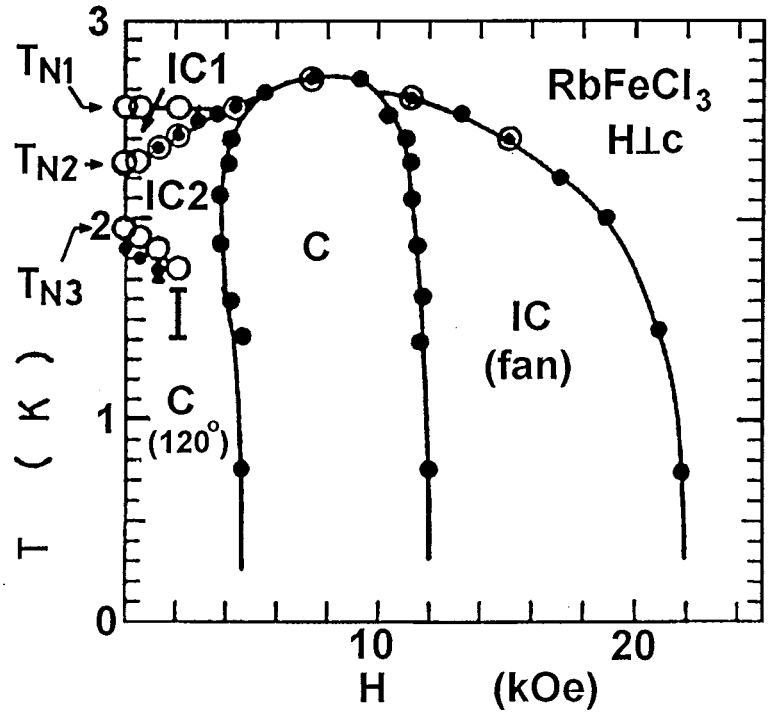

increases the phase-transition temperature until a maximum is reached at 7.5 T; subsequently there is a rapid decrease and the transition temperature goes to zero at 13 T. Shiba and Suzuki [225] propose a theory, which explains the experimental phase diagram reasonably well from the viewpoint of a conical-point instability due to the dipole–dipole interaction. They show that even a small dipole–dipole interaction can transform the 120° structure to an incommensurate structure at intermediate temperatures, although the low-temperature phase still should have the 120° structure. Very recently the phase diagram of $RbFeCl_3$ for $H \perp c$ was reinvestigated by neutron-scattering [235]. Good agreement between the results of two experiments was found for a field less than 1.0 T. Above 1.0 T the neutron-scattering study gives a slightly higher value of the transition field from the commensurate phase to the incommensurate phase.

The high field magnetization of $RbFeCl_3$ exhibits an anomaly around 31 T [236], similar to those in $CsFeCl_3$ [227]. The situation regarding the spin Hamiltonian parameters derived from experiment for $RbFeCl_3$ is very similar to that in $CsFeCl_3$. Different authors analyzed their experimental data on the basis of different approximations and there has been controversy about the value of the exchange interactions and the anisotropy. The results of a susceptibility measurements were analyzed using the molecular field approximation [237] or pair approximation [238], where a Fe^{2+} chain was represented by an assembly of isolated pairs of nearest neighbour spins. The Mössbauer and susceptibility data [200] were analyzed using the correlated effective-field approximation, developed by Lines [239]. The results of inelastic neutron-scattering [29] were analyzed using this theory, the three sublattice spin-wave approximation, and the exciton model. The parameters so determined

depend strongly on which approximation is used; they are not universal; one set of parameters cannot describe all available experimental data. Suzuki [213] has made an attempt to see to what extent one can understand the various observed magnetic properties on the basis of a single set of parameters. He used the dynamical correlated effective-field approximation [240] and has found values of $D, J_\perp, J_\parallel, g_\perp$, and $g_\parallel$, which can reproduce experimental data reasonably well. Originally he considered only a single chain of Fe^{2+} ions for the sake of simplicity, so that the approach is applicable only in the paramagnetic phase. Later he included an interchain coupling in the model and derived a consistent set of exchange parameters that explain the behaviour of $RbFeCl_3$ above and below T_N [241, 242].

5. Triangular antiferromagnet stacked ferromagnetically

Except for $CsFeCl_3$ and $RbFeCl_3$ as described in the previous chapter, there are just two triangular antiferromagnets with ferromagnetic interactions along the chains, $CsCuCl_3$ and $CsNiF_3$. Each gives rise to its own different physics, and will be dealt with in separate subsections of this chapter.

5.1. $CsCuCl_3$

$CsCuCl_3$ has been one of the most extensively studied of the triangular antiferromagnets. The spins in the copper chains are coupled ferromagnetically, but the planar interactions are antiferromagnetic so that frustration effects are of similar importance to the common case of antiferromagnetic chains.

What makes $CsCuCl_3$ unique is that below 423 K the triangular crystal structure is distorted through the Jahn–Teller effect to give a crystal structure with space group $P6_122$ [243, 244]. The distortion from the stacked triangular lattice involves small in-plane displacements of copper atoms so as to form a helix with axis along c with one turn of the helix every six layers.

Below T_N=10.66(1) K [245], the zero-field magnetic structure shows ab planes with the $120°$ triangular antiferromagnetic structure and with moments in the plane. Magnetic neutron Bragg peaks are observed at $(\frac{1}{3}\ \frac{1}{3}\ 6n\pm\delta)$ with δ=0.085 [34]. This corresponds to the triangular spin arrays that are rotated about c by $5.1°$ between successive planes. The period of rotation is $11.8c$ or 214 Å.

It is believed [34] that this rotation arises from the Dzyaloshinsky–Moriya (DM) interaction that gives rise to a term in the Hamiltonian given by

$$\mathcal{H}_{DM} = \sum_{i,j} \boldsymbol{D}_{ij} \cdot (\boldsymbol{S}_i \times \boldsymbol{S}_j) \tag{18}$$

In $CsCuCl_3$ $\boldsymbol{D}_{ij}$ is a vector along c, which is nonzero only when atoms i and j are nearest neighbours along the helical chains. In the absence of the Jahn–Teller distortion, symmetry requires the DM term to vanish; this is why it has not been included in the Hamiltonian for other materials discussed in this work. The Jahn–Teller distortion gives a second, smaller, effect on the Hamiltonian in that it causes the vector $\boldsymbol{D}_{ij}$ to deviate slightly from from the c axis with a period of six lattice spacings [34, 246]. This effect is small and often neglected in the literature. Neutron-scattering measurements of the spin-wave dispersion relations by Mekata et al. [245] confirm this Hamiltonian and give the intrachain exchange $J = -580$ GHz, $|D| = 121$ GHz and the in-plane exchange interaction $J' = 97$ GHz (no quantum corrections were included in deriving these parameters). It is apparent that $CsCuCl_3$ is less one dimensional than is usual for ABX_3 materials, since $|J/J'|$ is about 6 and in other materials it is one to two orders of magnitude larger.

The ferromagnetic interactions along the chain give a minimum energy when all the moments are aligned parallel, but the DM interaction is minimized when neighbouring moments are aligned perpendicularly. The sum of these two terms in the Hamiltonian gives a minimum energy classically for a helical magnet with the tangent of the turn angle between neighbouring moments equal to $|D/2J|$ [34]. The observed magnetic structure corresponds to these helices along c stacked on a

120° triangular lattice. The parameter δ is observed to be independent of temperature [34] and field ($H < H_c$) [247]. Spin-wave dispersion relations have been calculated by Rastelli and Tassi [248] and Stefanovskii and Sukstanskii [249] and are shown to agree with antiferromagnetic resonance data.

The maximum ordered moment for $S = \frac{1}{2}$ and $g = 2.10$ [250] is 1.05 μ_B. Adachi et al. [34] reported the ordered moment as (0.61 ± 0.01) μ_B, extrapolated to 0 K, but recent work gives higher values, 0.85 μ_B [245] for zero field and low temperature, and (0.90 ± 0.01) μ_B at $T = 10.35$ K and $H = 5.9$ T [247]. The two latter values are higher than is typical for frustrated systems, perhaps because the ferromagnetic chain coupling leads to smaller moment reductions than does antiferromagnetic coupling.

An applied field along c gives rise to two first-order phase transitions at fields H_{c1} and H_{c2}. Nojiri et al. [251] gives $H_{c1} = 12.5$ T and $H_{c2} = 31$ T at $T = 1.1$ K, while Chiba et al. [252] gives $H_{c1} = 11.19$ T at $T = 4.2$ K. For fields less than H_{c1} the magnetic structure is that found in zero field together with a canting of each spin towards the direction of the applied magnetic field. At H_{c1} the triangular layers break down into a colinear structure on the triangular lattice based on that shown in Fig. 11, where two spins are aligned in one direction and the third is in the opposite direction. There is a canting of all three spins towards the field direction [253]. The helical stacking of the planes remains in this structure. Neutron-scattering work [247] confirms this description of the magnetic structure above H_{c1}. On passing from the low-field to the medium-field structure the ($\frac{n}{3}$ $\frac{n}{3}$ $6l \pm \delta$) lines lose intensity and new lines appear at ($\frac{n}{3}$ $\frac{n}{3}$ $6l$). Above H_{c2} the magnetic structure is believed to be almost ferromagnetic, with the helical stacking destroyed. The phase transition at H_{c1} is not predicted for a classical system with the appropriate Hamiltonian; Nikuni and Shiba [253] show however that when quantum fluctuations are taken into account the phase transition is to be expected.

The field H_{c1} decreases slowly as the temperature increases [247, 254–256], and this line of first-order phase transition in the H–T phase diagram meets the paramagnetic phase transition at a bicritical point. Extrapolation of the neutron-scattering measurements of Stuesser et al. [247] indicate that the bicritical point occurs at $H_B = 5.5$ T and $T_B = 10.7$ K, while the specific-heat measurements of Weber et al. [256] give the same value for H_B and T_B = 10.59 K.

The behaviour of $CsCuCl_3$ in a field perpendicular to the c axis has been treated theoretically by Jacobs et al. [257, 258]. The field splits the degeneracy of the orientation of the spin triangle in the ab plane and causes the triangles to no longer have angles of 120°. This results in δ varying with the applied field H. An anomaly is observed [251] in the low-temperature magnetization at 12 T which is believed to involve a transition to a commensurate state. Since $CsCuCl_3$ is a frustrated system with $S = \frac{1}{2}$, quantum fluctuations would be expected to be important. Jacobs et al. [257] confirm this by evaluating the first term in a $1/S$ expansion and showing that quantum (and thermal) fluctuations lift a nontrivial degeneracy and stabilize the commensurate state.

We finish this subsection by describing work on the critical phase transition. The magnetism in $CsCuCl_3$ shows two chiral degeneracies, one arising from the triangular structure in each plane and one from the helix along the c axis. Weber et al. [256] argue that the structural helix will not affect the critical properties and that the phase transition should be that of the chiral XY model. This model predicts $\beta = 0.25 \pm 0.01$ and $\alpha = 0.34 \pm 0.06$ (Table 5), while if the nonuniversality model holds tricritical exponents would be observed with $\beta = 0.25$ and $\alpha = 0.5$ (Table 3). The early neutron-scattering measurements of Adachi et al. [34] gave $\beta = 0.358 \pm 0.015$, but this value has not been confirmed by recent work that gives much lower values; Mekata et al. [245] give 0.25 ± 0.01 and Stuesser et al. [247] give 0.23 ± 0.02. Recent specific-heat measurements of Weber et al. [256] in zero field can be described well by a critical exponent $\alpha = 0.35 \pm 0.05$ except very close to T_N ($t < 10^{-3}$) where the transition seems to go over to being weakly first order. The exponent is compatible with the chiral XY model and not with the tricritical model. The small canting of the vector $\boldsymbol{D}_{ij}$ from the c axis will lower the symmetry from $Z_2 \times S_1$ to Z_2. Thus the critical properties should eventually

Fig. 18. Spin arrangement in the ab plane for $CsNiF_3$. The unit cell is orthorhombic as shown by the continuous lines.

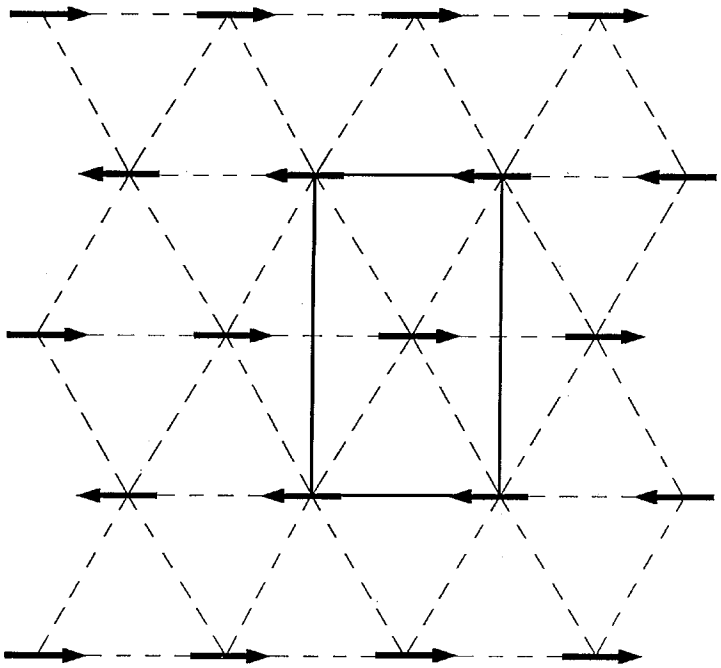

exhibit a crossover effect from $Z_2 \times S_1$ to Z_2 behaviour, though this effect has not been observed to date. It is not clear whether the observed weakly-first-order effects are a fundamental property of the frustrated XY model or if they are a consequence of the expected crossover.

As the field increases towards H_{B} the amplitude of the specific-heat divergence becomes smaller and the first order part of the transition becomes even weaker. At a field above H_{B}, $H = 7$ T, the specific-heat measurements show a critical phase transition with $\alpha = 0.23 \pm 0.08$, contrary to the expected value for regular XY behaviour where $\alpha = -0.01$. The origin of this discrepancy is not clear.

5.2. $CsNiF_3$

This is the only fluoride ABX_3 compound that crystallizes with the stacked triangular lattice [259]. The magnetic structure corresponds to an easy-plane antiferromagnet with no distortions at low temperatures. As usual the interactions are much stronger along c than within the ab plane, giving rise to quasi-one-dimensional properties above T_N. The interactions along the chain and the soliton properties have been much studied in the quasi-one-dimensional temperature region (see Kakurai et al. [260] and references therein). In this article only the three-dimensional ordered properties will be discussed. These are unique for an easy-axis material since the ordering consists of ferromagnetic ac planes stacked antiferromagnetically with moments aligned along a [261], as shown in the Fig. 18.

This ordering implies that the low-temperature ordered state breaks the hexagonal symmetry. In practice domains are formed favouring one of the three equivalent a directions in the basal plane. In terms of the hexagonal unit cell, Bragg peaks are observed in the low-temperature neutron-scattering pattern with indices $(h/2, k, l)$ where h, k, and l are all integers.

The magnetic order cannot arise from a Hamiltonian containing just nearest-neighbour interactions and easy-plane anisotropy, as has been shown in earlier chapters. Scherer and Barjhoux [262] and

Table 11. Various determinations of the magnetic parameters J, J', D and T_N for $CsNiF_3$.

Experimental technique	$-J$ (GHz)	J' (GHz)	D (GHz)	T_N (K)
Neutron-scattering	239(2) [266]		185(4) [266]	2.67(5) [261]
				2.664 [267]
Specific-heat	173(17) [268]			2.613(3) [268]
Magnetization	208(10) [269]		177(10) [269]	
	270 [262]	0.71 [262]		
AFMR	245 [263,270]		191(10) [263,270]	2.61 [263,270]
Ultrasonic velocity				2.77(1) [271]

Suzuki [263] show that it will occur if the interactions, other than those along the chains, are predominantly dipolar in character. The idea of this predominance is supported by the low value of the Néel temperature, 2.7 K, which shows weak interchain interactions. The value of the ordered moment, 2.26 μ_B [261], for $S = 1$ and $g = 2.28$, is higher than is found in frustrated triangular structures. A theoretical treatment that includes magnetoelastic effects has been given by Caillé and Plumer. A mean-field treatment of the phase diagram is given by Trudeau and Plumer [264].

The various experimentally-determined values of J, J', D, and T_N are listed in the Table 11. It is clear that the in-plane exchange, J', is small compared with the exchange along the chains, J, but the magnitude is similar to that found in other ABX_3 easy-plane materials (see Table 2). The anisotropy, D, is however larger than in other easy-axis materials. The dipolar forces are long range in nature and their relative influence, which comes from sums over a large number of moments, is greater for ferromagnetic than for antiferromagnetic chain interactions. Theory [262, 263, 265] predicts the correct structure for the parameters given in Table 11 together with dipolar interactions.

Because the chains are ferromagnetic, it would be expected that applied magnetic fields will have a relatively greater influence than in other ABX_3 materials. This is indeed the case for fields applied in the basal plane, though the strong easy-plane anisotropy makes the effect of fields applied along c less.

The neutron-scattering measurements of Steiner and Dachs [272] show that small fields, H, applied in the basal plane to the ordered material influence the relative sizes of the three domains. A field of around 0.05 T is sufficient to produce a single-domain sample with moments approximately perpendicular to H. Larger fields destabilize the antiferromagnetic state and there is a phase transition at critical field, H_c, to a paramagnetic state with imposed alignment of the moments along H. H_c is around 0.2 to 0.3 T at 2.0 K [271,272]

If the field is applied along c, larger values of H are needed to destroy the antiferromagnetism because the field is opposed by the easy-plane anisotropy. A similar phase transition occurs in this case, but the critical field, H_c is 8 to 25 times larger than when H is applied in the basal plane [265,271].

The critical properties of $CsNiF_3$ are not simple. The Hamiltonian has XY symmetry in zero field or with applied field $H < H_c$ along c. For an applied field in the plane sufficient to produce a single-domain sample the symmetry becomes Ising like [273] with z in a direction perpendicular to both c and H. There are two complicating factors however. First, the long-range nature of the dipolar interactions can lead to mean-field exponents and to crossover behaviour. Second, the presence of three equivalent domains in the structure changes the critical properties and makes the phase transition first order [274].

Neutron-scattering measurements in zero field [267] show a critical phase transition with a crossover at $t = |T - T_c|/T_c$ values near 1.3×10^{-2} from exponents, $\gamma = 1.1 \pm 0.1$ and $\nu = 0.54 \pm 0.07$, at large t, to different values, $\gamma = 1.45 \pm 0.10$, $\nu = 0.68 \pm 0.07$ and $\beta = 0.34 \pm 0.04$, at small t. Although the errors on the exponents are not small, the first set is consistent with mean-field

exponents and the second set with XY behaviour. There is no experimental evidence for a first-order phase transition. Strain effects have been observed in $CsNiF_3$ crystals [271] which might suppress domain fluctuations, but this would not be expected to completely change the nature of the transition.

There is one other set of measurements of critical properties. Lussier and Poirier [271] have measured the phase boundary H_c as a function of temperature and of the direction of H. For fields perpendicular to c, H_c is large enough for the sample to be single domain and Ising symmetry is to be expected. Plumer and Caillé [265] show that H_c varies as the order parameter, so that the measurements should result in an Ising critical exponent $\beta = 0.326$. The measured exponent is 0.31 ± 0.01 in not-too-bad agreement with theoretical expectations. The situation with H along c is puzzling however. Theory predicts an XY exponent, $\beta = 0.345$, for H_c while the experiment gives a higher value, $\beta = 0.37 \pm 0.01$.

6. Diluted and mixed triangular magnets

It is apparent from previous chapters (or at least the authors hope it is apparent) that there are plenty of triangular magnets, the physical properties of which depend on the type and relative strength of the exchange and anisotropic interactions. Those properties are not totally established yet. Even less understanding of properties of diluted and mixed triangular magnets is currently achieved—as they are found to be much more sophisticated ; nevertheless, some interesting results have been found and ideas formulated in the process of their investigation. It is useful to draw the analogy here between the triangular antiferromagnets and another example of a frustrated magnetic system, the XY square-lattice antiferromagnet dominated by second-neighbour antiferromagnetic exchange. In the latter case dilution acts against thermal and quantum fluctuations, producing an effect known as "ordering due to disorder" [275]. The present chapter summarizes briefly the characteristics of diluted and mixed magnets on a triangular lattice.

The obvious method to "disturb" the magnetic system is to introduce small amounts of nonmagnetic impurities. The presence of an impurity results either in mechanical distortion of the structure of the original crystal or in the disruption of some part of the interaction between the magnetic atoms, which is reflected in the collective behaviour of the spin system. The random field effect due to the nonmagnetic impurities on spin correlation was studied by elastic neutron-scattering and magnetic susceptibility measurements in an Ising antiferromagnet, $CsCoCl_3$, doped by Mg or Zn [276] and by measurements of diffuse scattering in $CsCoCl_3$ doped by Mg [172]. The reduction of the upper magnetic transition temperature, T_{N1}, has been found in samples with impurities: $T_{N1} = 21.0$ K for the pure crystal, $T_{N1} = 20.3$ K crystal with 0.58% of Mg , for a $T_{N1} = 19.8$ K and crystal with 1.7% of Mg, respectively [172], while the temperature of the lower magnetic transition, T_{N2}, could not be found down to 1.6 K [276]. The Mg concentration was determined by a chemical analysis.

On the other hand, detailed ESR and magnetization measurements of Heisenberg triangular antiferromagnet, $RbNiCl_3$, doped with 1% of Mg showed that the Neél temperature remained unchanged from pure crystal, in which $T_N \approx 11$ K [277]. However, the influence of the impurity at low temperature is still well pronounced:

(1) the spin-flop region became much broader,

(2) the gap $\omega(H = 0)$ of one of the resonance branches has increased from 55 to 61 GHz,

(3) the gap of another resonance branch has found to be 20 GHz, while in the pure crystal it was not been observed and its estimated value is 0.2 GHz.

Such a dramatic changing of the resonance spectrum was successfully described by introducing a two-ion anisotropy of the form $D(S_i^z)^2(S_j^z)^2$ into the spin Hamiltonian (1). It has been postulated that an impurity that does not occupy a site in the crystal lattice strongly distorts the electrical interactions within the crystal, altering the character of the anisotropic interactions. In contrast to the case of doped $CsCoCl_3$, where the Mg concentration was different in different crystals, a γ activation

Fig. 19. Magnetic phase diagrams of $CsNi_{0.98}M_{0.02}Cl_3$, after Trudeau et al. [282] Reprinted with permission from the publisher.

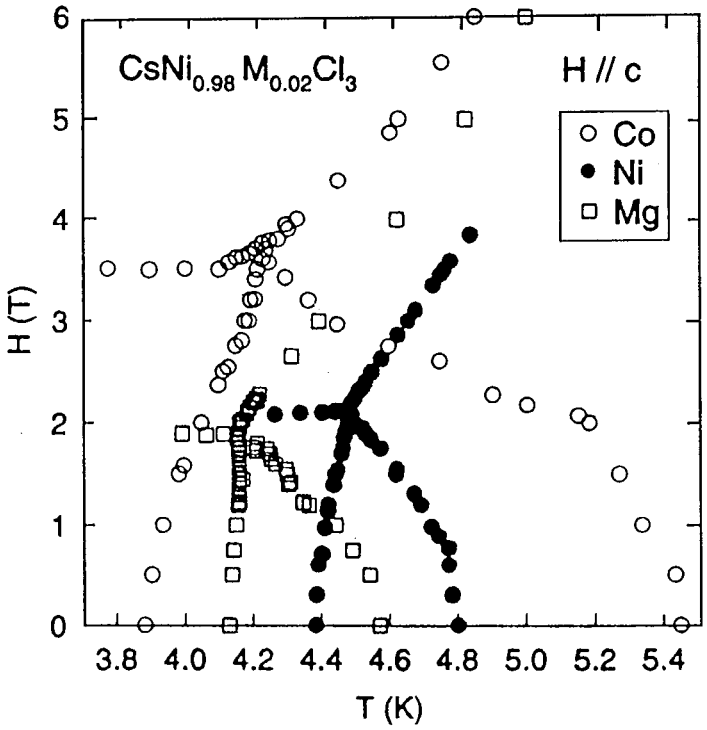

analysis revealed approximately the same concentration (about 1%) of Mg in all the crystals of $RbNiCl_3$ investigated.

A very unusual result has been reported recently by Yamazaki et al. [278] for a $CsV_{1-x}Mg_xCl_3$, ($x = 0.000 - 0.357$). The temperature-dependence of the magnetic susceptibility for a sample with $x = 0.026$ suggests that the ordering temperature is about 35 K, while in a pure sample $T_{N1} = 13.8$ K [32]. Such a dramatic increase of the ordering temperature obviously has to be confirmed by some other techniques.

The influence of diamagnetic dilution on the magnetic ordering process of the induced-moment antiferromagnet $RbFeCl_3$ is studied in ref. 279. Single crystals of the solid solution $RbFe_{1-x}Mg_xCl_3$ ($x = 0.02$, 0.03 and 0.05) were investigated by means of elastic neutron-scattering. The $x = 0.02$ and 0.03 samples showed transitions from paramagnetic to the IC_1 phase at the same temperature, $T_{N1} = 2.55$ K (see Fig. 17), then transitions to the IC_2 and C phases at temperatures that decreased sharply with x. The $x = 0.05$ sample also shows a transition to the IC_1 phase at $T_{N1} = 2.55$ K, but no further transitions down to the lowest temperature of 1.38 K. An additional elastic diffuse magnetic-scattering component centred at the vector $(\frac{1}{3}\frac{1}{3}0)$ has been found to persist to temperatures well above T_N in all samples.

Another method of investigation of the magnetic system consists of introducing small amount of magnetic impurities. A substitution of magnetic ions can modify the amplitude, or even sign, of the effective single-ion anisotropy. For example, in pure $RbNiCl_3$ the splitting between T_{N1} and T_{N2} is very small, 0.14 T [110], while addition of only 5% of Co results in as much as 9 K between T_{N1} and T_{N2} [280]. Magnetic phase diagrams of the Heisenberg triangular antiferromagnet, $CsNi_{0.98}M_{0.02}Cl_3$ (M = Co, Fe, Mg) have been determined by heat capacity [281] and ultrasonic velocity [282] mea-

surements. As expected, when comparing with pure $CsNiCl_3$, the Co-doped crystal shows enhanced Ising effective single-ion anisotropy—the spin-flop field H_{SF} and the splitting between T_{N1} and T_{N2} are sufficiently increased; the Fe-doped crystal behaves as a Heisenberg antiferromagnet with the XY type of anisotropy—the phase diagram is very similar to those in $CsMnBr_3$; in the Mg-doped crystal nonmagnetic impurity causes decrease of effective single-ion anisotropy and values of H_{SF} and T_N consequently. Magnetic phase diagrams of $CsNi_{0.98}M_{0.02}Cl_3$ for H parellel to c is shown on Fig. 19.

Apart from the addition of small amounts of impurities into antiferromagnets on a triangular lattice, some investigations had been done on mixed systems, where the impurity concentration is not small. In ref. 283 the magnetic phase diagram of $Rb_{1-x}K_xNiCl_3$ has been studied by susceptibility and torque measurements. Pure $RbNiCl_3$ is a Heisenberg antiferromagnet with easy-axis type anisotropy, while $KNiCl_3$ demonstrates large easy-plane type anisotropy, see Chap. 2. The transition between two different types of anisotropy has been found at $x_c = 0.38$. The interpretation of the observed phase diagram at large x is quite complicated due to crystal structure distortions of pure $KNiCl_3$.

Harrison and coauthors [284–286] have investigated magnetic ordering effects in the mixed singlet-ground-state magnets $AFeX_3$, where A is a mixture of Cs and Rb or X is the mixture of Cl and Br. As was shown in Chap. 4 $CsFeCl_3$ has a "truly" nonmagnetic ground state, while in $RbFeCl_3$ sufficiently strong exchange interaction causes magnetic ordering at $T < T_N = 2.5$ K. Therefore, the replacement of Rb in $RbFeCl_3$ by Cs should decrease Neél temperature or even suppress magnetic ordering. Indeed, it was found experimentaly [284], that as low as 5% of Cs is sufficient to destroy long-range magnetic ordering. In $RbFeCl_{3-x}Br_x$, there is an obvious competition between the ferromagnetic and antiferromagnetic sign of the intrachain interactions: in $RbFeCl_3$ the exchange along c axis is ferromagnetic, while in $RbFeBr_3$ it is antiferromagnetic (see Chap. 4). Again, low concentrations of either type of dopant, $0.3 < x < 2.7$, destroys the magnetic long-range order [285]. Note, that at intermediate compositions a singlet ground-state phase has been observed, rather than the expected spin-glass phase.

7. Conclusions

As was mentioned in the Introduction, there are several ways that triangles of antiferromagnetic interactions can be built into a crystal lattice. The distinguishing feature of the majority of antiferromagnets on a stacked triangular lattice, described in this article, is the appearance at sufficiently low temperatures of the three-dimensional long-range magnetic ordering, despite the frustration of the exchange interaction. The transition temperature of this sort of antiferromagnets is typically an order of magnitude lower than the Curie–Weiss temperature, but such a big reduction of the transition temperature usually arises from a combination of two effects, frustration and the low-dimensionality of actual stacked-triangular materials (they have quasi 1D or 2D character).

The influence of the frustration on the magnetic properties of other triangular antiferromagnets, which have more complicated structures, is apparently more substantial. For example, in Kagome-lattice antiferromagnet $SrCr_{9p}Ga_{12-9p}O_{19}$, with $p \approx 0.9$ [287], the low-temperature ground state is a spin glass. In gadolinium gallium garnet, $Gd_3Ga_5O_{12}$, where the magnetic Gd ions are on two interpenetrating corner-sharing triangular sublattices, long-range magnetic order has been found only in the applied magnetic field around 1 T [288], while in a lower field, magnetization is different for a field cooling and zero field cooling [289], which is typical for a spin glass. Many pyrochlores with the chemical formula $A_2B_2O_7$ also undergo a phase transition to a spin glass state [16].

Because triangular antiferromagnets on a stacked triangular lattice still can be described at low temperature in terms of Neél-type ordering, rather than spin-glass or a short-range order, they form a good basis for the study of the effects of frustration on magnetic systems. Frustration leads to new physics with novel phase diagrams and critical properties. Zero-point fluctuations are found in Ising systems; these become large in XY and Heisenberg systems.

Theory and experiment seem to be in good accord in describing the ground state and the excitations of the triangular antiferromagnets except in the case of $S = 1$ quasi-one-dimensional nickel materials where spin-wave theory seems to be inadequate. Correction terms for ground-state fluctuations are larger than can be dealt with confidently and vestiges of the one-dimensional Haldane effect are believed to be present.

Theoretical predictions of the nature of the phase diagram as a function of H and T are in accord with experiment, but the critical properties at phase transitions are often not described satisfactorily. For materials with the Heisenberg Hamiltonian, the theoretical consensus favours Kawamura's SO(3) chiral universality class, but experiments show significant discrepancies. For the XY Hamiltonian the theoretical situation is controversial with three contending scenarios, chiral XY properties, tricritical properties, and a weak first-order phase transition. Experiment, which is largely confined to one material, $CsMnBr_3$, shows a critical phase transition with exponents that can be taken to be in agreement with either the chiral XY model or tricritical exponents; the two theories give quite similar predictions for the exponents. There is a need for measurements of critical exponents of weak ($D < 3J'$) easy-plane materials and for strong easy-plane materials in a field.

For easy-axis materials the experimental values and the theoretical predictions for the critical indices β, ν, and γ at both of the two zero-field phase transitions are irreconcilable. The experimental values are not in accord with the scaling laws and a confirmation of the single report of values of ν and γ would be desirable.

A number of cobalt quasi-one-dimensional triangular antiferromagnets have Hamiltonians that are close to the Ising Hamiltonian. The zero-field properties of these materials is not simple with three phase transitions. Only the upper one of these shows a specific-heat anomaly. Most theoretical work has predicted critical exponents at the upper critical temperature that follow the three-dimensional unfrustrated XY model, and most experiments agree with these predictions. One recent Monte Carlo study suggested slightly different exponents, but unfortunately the experiments are not sufficiently accurate to distinguish. One group has recently reported experimental determinations of β that are significantly lower than those given in other reports, and that are not in accord with any theoretical predictions.

It has long been a puzzle as to why one triangular antiferromagnet, $RbMnBr_3$ shows an incommensurate magnetic structure. Recently we and our coworkers have shown that this arises from small structural distortions of the lattice along planes perpendicular to the basal plane. These distortions, which map on to the row model of Zhang, et al., allow relatively small changes in exchange parameters, arising from the distortions, to destroy the simple triangular magnetic structure. Similar distortion effects are also found in $KNiCl_3$.

Acknowledgments

We are grateful to Drs. R. Feyerherm, B.D. Gaulin, J. Gardner, M.L. Plumer, D. Visser, and M. Zhitomirsky for useful discussions about some aspects of this manuscript. We thank the Natural Sciences and Engineering Research Council of Canada for financial support. One of the authors (MFC) wishes to thank the Chalk River Laboratories for hospitality during a sabbatical visit while the this article was written.

References

1. H. Kawamura. J. Phys. Soc. Jpn. **56**, 474 (1987).
2. H. Kawamura. J. Phys. Soc. Jpn. **58**, 584 (1979).
3. H. Kawamura. J. Phys. Soc. Jpn. **61**, 1299 (1992).
4. T. Bhattacharya, A. Billoire, R. Lacaze, and T. Jolicoeur. J. Phys (Paris), **I4**, 122 (1994).
5. D. Loison and H.T. Diep. Phys. Rev. B: Condens. Matter, **50**, 16 453 (1994).
6. A. Mailhot, M.L. Plumer, and A. Caillé. Phys. Rev. B: Condens. Matter, **50**, 6854 (1994).

7. H. Kawamura. Phys. Rev. B: Condens. Matter, **38**, 4916 (1988).
8. P. Azaria, P. Delamotte, and T. Jolicoeur. Phys. Rev. Lett. **64**, 3175 (1990).
9. S.A. Antonenko and A.I. Sokolov. Phys. Rev. B: Condens. Matter, **49**, 15901 (1994).
10. H. Kadowaki, K. Ubukoshi, K. Hirakawa, J.L. Martinez, and G. Shirane. J. Phys. Soc. Jpn. **56**, 4027 (1987).
11. T.E. Mason, B.D. Gaulin, and M.F. Collins. Phys. Rev. B: Condens. Matter, **39**, 586 (1989)
12. B.D. Gaulin, T.E. Mason, M.F. Collins, and J.F. Larese. Phys. Rev. Lett. **62**, 1380 (1989).
13. D.H. Lee, J.D. Joannopoulos, J.W. Nagele, and D.P. Landau. Phys. Rev. Lett. **52**, 433 (1984); Phys. Rev. B: Condens. Matter, **33**, 450 (1986).
14. A.V. Chubukov and D.I. Golosov. J. Phys.: Condens. Matter, **3**, 69 (1991).
15. T. Momoi. J. Stat. Phys. **75**, 707 (1994).
16. B.D. Gaulin. *In* Magnetic systems with competing interactions. *Edited by* H.T. Diep. World Scientific, Singapore. 1994. p. 286.
17. M.L. Plumer, A. Caillé, A. Mailhot, and H.T. Diep. *In* Magnetic systems with competing interactions. *Edited by* H.T. Diep. World Scientific, Singapore. 1994. p. 1.
18. A.P. Ramirez. Annu. Rev. Mater. Sci. **24**, 453 (1994).
19. W.E. Hatfield, W.E. Estes, W.E. Marsh, M.W. Pickens, L.W. ter Haar, and R.R. Weller. Ext. Linear Chain Compd. **3**, 43 (1983).
20. S.R. Kuindersma, C. Haas, J.P. Sanchez, and R. Al. Solid State Commun. **30**, 403 (1979).
21. K. Hirakawa, H. Kadowaki, and K. Ubukoshi. J. Phys. Soc. Jpn. **52**, 1814 (1983).
22. T. Sato, H. Kadowaki, H. Masuda, and K. Iio. J. Phys. Soc. Jpn. **63**, 4583 (1994).
23. J.L. Soubeyroux, D. Fruchart, J.C. Marmeggi, W.J. Fitzgerald, C. Delmas, and G. Le Flem. Phys. Status Solidi, **67**, 633 (1981).
24. H. Kadowaki, H. Takei, and K. Motoya. J. Phys.: Condens. Matter, **7**, 6869 (1995).
25. H. Kadowaki, H. Kikuchi, and Y. Ajiro. J. Phys.: Condens. Matter, **2**, 4483 (1990).
26. Y. Oohara, S. Mitsuda, H. Yoshizawa, N. Yaguchi, H. Kuriyama, T. Asano, and M. Mekata. J. Phys. Soc. Jpn. **63**, 847 (1994).
27. H. Hori, H. Mikami, M. Date, and K. Amaya. Physica B, **165&166**, 237 (1990).
28. W.J. Crama. J. Solid State Chem. **39**, 168 (1981).
29. H. Yoshizawa, W. Kozukue, and K. Hirakawa. J. Phys. Soc. Jpn. **49**, 144 (1980).
30. M. Melamud, J. Makovsky, H. Shaked, and S. Shtrikman. Phys. Rev. B: Solid State, **3**, 821 (1971).
31. W.B. Yelon and D.E. Cox. Phys. Rev. B: Solid State, **6**, 204 (1972).
32. A. Hauser, U. Falk, P. Fischer, and H. Gudel. J. Solid State Chem. **56**, 343 (1985).
33. M. Mekata and K. Adachi. J. Phys. Soc. Jpn. **44**, 806 (1978).
34. K. Adachi, N. Achiwa, and M. Mekata. J. Phys. Soc. Jpn. **49**, 545 (1980).
35. M. Melamud, J. Makovsky, and H. Shaked. Phys. Rev. B: Solid State, **3**, 3873 (1971).
36. V.J. Minkiewicz, D.E. Cox, and G. Shirane. Solid State Commun. **8**, 1001 (1970).
37. V.J. Minkiewicz, D.E. Cox, and G. Shirane. J. Phys. (Paris) C, **1** C1 (1971).
38. A. Harrison and D. Visser. J. Phys.: Condens. Matter, **4**, 6977 (1992).
39. C.J. Glinka, V.J. Minkiewicz, D.E. Cox, and C.P. Khattak. Magnetism and Magnetic Materials. 18th Ann. Conf. 659 (1973).
40. H.T. Witteveen and J.A.R. van Veen. J. Phys. Chem. Solids, **35**, 337 (1974).
41. W.B. Yelon, D.E. Cox, and M. Eibschutz. Phys. Rev. B: Solid State, **12**, 5007 (1975).
42. B. Dorner, D. Visser, U. Steigenberger, K. Kakurai, and M. Steiner. Z. Phys. B: Condens. Matter, **72**, 487 (1988).
43. M. Eibshütz, R.C. Sherwood, F.C.L. Hsu, and D.E. Cox. AIP Conf. Proc. **10**, 684 (1973).
44. R. Brener, E. Ehrenfreund, H. Shechter, and J. Makovsky. J. Phys. Chem. Solids, **38**, 1023 (1977).
45. H.W. Zandbergen. J. Solid State Chem. **37**, 308 (1981).
46. H.W. Zandbergen. Ph.D. thesis, University of Leiden. 1981.
47. H.W. Zandbergen. J. Solid State Chem. **35**, 367 (1980).
48. H. Tanaka, Y. Kaahwa, T. Hasegawa, M. Igarashi, S. Teraoka, K. Iio, and K. Nagata. J. Phys. Soc. Jpn. **58**, 2930 (1989).
49. O.A. Petrenko, M.F. Collins, C.V. Stager, and Z. Tun. Phys. Rev. B: Condens. Matter, **51**, 9015 (1995).
50. M. Steiner, W. Kruger, and D. Babel. Solid State Commun. **9**, 227 (1971).

51. H. Tanaka, K. Iio, and K. Nagata. J. Magn. Magn. Mater. **104–107**, 829 (1992).
52. R.M. Morra, W.J.L. Buyers, R.L. Armstrong, and K. Hirakawa. Phys. Rev. B: Condens. Matter, **38**, 543 (1988).
53. K. Katori, Y. Ajiro, T. Asano, and T. Goto. J. Phys. Soc. Jpn. **64**, 3038 (1995).
54. I.A. Zaliznyak, L.A. Prozorova, and A.V. Chubukov. J. Phys.: Condens. Matter, **1**, 4743 (1989).
55. K. Kakurai. Physica B, **180–181**, 153 (1992).
56. Z. Tun, W.J.L. Buyers, A. Harrison, and J.A. Rayne. Phys. Rev. B: Condens. Matter, **43**, 13331 (1991).
57. E. Cohen and M.D. Sturge. Solid State Commun. **24**, 51 (1977).
58. K. Nakajima, K. Kakurai, H. Hiraka, H. Tanaka, K. Iio, and Y. Endoh. J. Phys. Soc. Jpn. **61**, 3355 (1992).
59. O.A. Petrenko, S.V. Petrov, and L.A. Prozorova. Sov. Phys. JETP, **71**, 406 (1990).
60. K. Iio, M. Sano, and K. Nagata. J. Magn. Soc. Jpn. **11**,(Suppl. 59) (1987).
61. S. Maegawa, T. Kohmoto, and T. Goto. Phys. Rev. B: Condens. Matter, **44**, 12617 (1991).
62. A. Harrison, M.F. Collins, J. Abu-Dayyeh, and C.V. Stager. Phys. Rev. B: Condens. Matter, **43**, 679 (1991).
63. T. Inami, K. Kakurai, H. Tanaka, M. Enderle, and M. Steiner. J.Phys. Soc. Jpn. **63**, 1530 (1994).
64. Z .Tun, T.C. Hsu, and J-G. Lussier. J. Appl. Phys. **75**, 6063 (1994).
65. M. Enderle, K. Kakurai, K.N. Clausen, T. Inami, H. Tanaka, and M. Steiner. Europhys. Lett. **25**, 17 (1993).
66. S.I. Abarzhi, M.E. Zhitomirsky, O.A. Petrenko, S.V. Petrov, and L.A. Prozorova. Sov. Phys. JETP, **77**, 521 (1993).
67. M.F. Collins and B.D. Gaulin. J. Appl. Phys. **55**, 1869 (1984).
68. B.D. Gaulin, M.F. Collins, and W.J.L. Buyers. J. Appl. Phys. **61**, 3409 (1987).
69. U. Falk, A. Furrer, H.U. Gudel, and J.K. Kjems. Phys. Rev. B: Condens. Matter, **35**, 4888 (1987).
70. T. Inami, K. Kakurai, H. Tanaka, M. Enderle, and M. Steiner. Physica B, **213&214**, 167 (1995).
71. L. Heller, M.F. Collins, Y.S. Yang, and B. Collier. Phys. Rev. B: Condens. Matter, **49**, 1104 (1994).
72. A.G. Abanov and O.A. Petrenko. Phys. Rev. B: Condens. Matter, **50**, 6271 (1994).
73. M. Niel, C. Cros, M. Pouchard, and J.-P. Chaminade. J. Solid State Chem. **20**, 1 (1977).
74. R. Feile, J.K. Kjems, A. Hauser, H.U. Gudel, U. Falk, and A. Furrer. Solid State Commun. **50**, 435 (1984).
75. H. Tanaka and K. Kakurai. Physica B, **213&214**, 188 (1995).
76. H. Tanaka and K. Kakurai. J. Phys. Soc. Jpn. **63**, 3412 (1994).
77. H. Kadowaki, K. Hirakawa, and K. Ubukoshi. J. Phys. Soc. Jpn. **52**, 1799 (1983).
78. S. Itoh, Y. Endoh, K. Kakurai, and H. Tanaka. Phys. Rev. Lett. **74**, 2375 (1995); Physica B, **213&214**, 161 (1995).
79. M. Niel, C. Cros, G. Le Flem, M. Pouchard, and P. Hagenmuller. Physica B, **86–88**, 702 (1977).
80. I. Yamada, K. Ubukoshi, and K. Hirakawa. J. Phys. Soc. Jpn. **53**, 381 (1984).
81. H. Kadowaki, K. Ubukoshi, and K. Hirakawa. J. Phys. Soc. Jpn. **54**, 363 (1985).
82. C. Delmas, F. Menil, G. Le Flem, C. Fouassier, and P. Hagenmuller. J. Phys. Chem. Solids, **39**, 51 (1978); C. Delmas, G. Le Flem, C. Fouassier, and P. Hagenmuller. J. Phys. Chem. Solids, **39**, 55 (1978).
83. S. Angelov, J. Darriet, C. Delmas, and G. Le Flem. Solid State Commun. **50**, 345 (1984).
84. J.-P. Doumerc, A. Wichainchai, A. Ammar, M. Pouchard, and P. Hagenmuller. Mater. Res. Bull. **21**, 745 (1986).
85. D. Juza, D. Giegling, and H.Schäfer. Z. Anorg. Allgem. Chem. **366**, 121 (1961).
86. K. Takeda, N. Uryu, K. Ubukoshi, and K. Hirakawa. J. Phys. Soc. Jpn. **55**, 727 (1986).
87. J. Wosnitza, R. Deutschmann, H. v Lohneysen, and R.K. Kremer. J. Phys.: Condens. Matter, **6**, 8045 (1994).
88. F. Tabak, A. Lascialfari, and A. Rigamonti. J. Phys.: Condens. Matter, **5**, B31 (1993).
89. M. Nishi, Y. Ito, H. Kadowaki, and K. Hirakawa. J. Phys. Soc. Jpn. **53**, 1214 (1984).
90. M.F. Collins. Magnetic critical scattering. Oxford University Press, Oxford. 1989.
91. N. Kojima, K. Ito, I. Mogi, M. Takeda, G. Kido, Y. Nakagawa, M. Sakai, N. Kuroda, and Y. Nishina. J. Phys. Soc. Jpn. **62**, 4137 (1993).
92. M. Suzuki, I. Yamada, H. Kadowaki, and F. Takei. J. Phys.: Condens. Matter, **5**, 4225 (1993)
93. Y. Ajiro, H. Kikuchi, S. Sugiyama, T. Nakashima, S. Shamoto, N. Nakayama, M. Kiyama, N. Yamamoto,

and Y. Oka. J. Phys. Soc. Jpn. **57**, 2268 (1988).
94. J.L. Soubeyroux, D. Fruchart, C. Delmas, and G. Le Flem. J. Magn. Magn. Mater. **14**, 159 (1979).
95. S. Angelov and J.P. Doumerc. Solid State Commun. **77**, 213 (1991).
96. H. Kawamura and S. Miyashita. J. Phys. Soc. Jpn. **53**, 4138 (1984).
97. K. Hirakawa, H. Kadowaki, and K. Ubukoshi. J. Phys. Soc. Jpn. **54**, 3526 (1985).
98. H. Kadowaki, K. Ubukoshi, and K. Hirakawa. Unpublished. Cited in ref. 81.
99. R.H. Clark and W.G. Moulton. Phys. Rev. B: Solid State, **5**, 788 (1972).
100. D. Beckmann, J. Wosnitza, H von Lohneysen, and D. Visser. Phys. Rev. Lett. **71**, 2829 (1993).
101. P.B. Johnson, J.A. Rayne, and S.A. Friedberg. J. Appl. Phys. **50**, 1853 (1979).
102. H. Kadowaki, K. Ubukoshi, and K. Hirakawa. J. Phys. Soc. Jpn. **56**, 751 (1987).
103. D.E. Cox and V.J. Minkiewicz. Phys. Rev. B: Solid State, **4**, 2209 (1971).
104. W.B. Yelon and D.E. Cox. Phys. Rev. B: Solid State, **7**, 2024 (1972).
105. M. Poirier, A. Caillé, and M.L. Plumer. Phys. Rev. B: Condens. Matter, **41**, 4869 (1990).
106. I.A. Zaliznyak, V.I. Marchenko, S.V. Petrov, L.A. Prozorova, and A.V. Chubukov. JETP Lett. **47**, 211 (1988).
107. H. Tanaka, S. Teroaka, E. Kakehashi, K. Iio, and K. Nagata. J. Phys. Soc. Jpn. **57**, 3979 (1988).
108. T. Kambe, H. Tanaka, S. Kimura, H. Ohta, M. Motokawa, and K. Nagata. J. Magn. Magn. Mater. **140–144**, 1967 (1995).
109. Y. Trudeau, M.L. Plumer, M. Poirier, and A. Caillé. Phys. Rev. B: Condens. Matter, **48**, 12805 (1993).
110. Y. Oohara, H. Kadowaki, and K. Iio. J. Phys. Soc. Jpn. **60**, 393 (1991).
111. H.A. Katori, T. Goto, and Y. Ajiro. J. Phys. Soc. Jpn. **62**, 743 (1993).
112. M. Sano, K. Iio, and K. Nagata. Phys. Rev. B: Condens. Matter, **39**, 9753 (1989).
113. H. Kadowaki, T. Inami, Y. Ajiro, K. Nakajima, and Y. Endoh. J. Phys. Soc. Jpn. **60**, 1708 (1991).
114. M. Enderle, G. Fortuna, and M. Steiner. J. Phys.: Condens. Matter, **6**, L385 (1994).
115. Y. Ajiro, T. Inami, and H. Kadowaki. J. Phys. Soc. Jpn. **59**, 4142 (1990).
116. T. Oguchi. Phys. Rev. **117**, 117 (1960).
117. P-A. Lindgard and A. Kowalska. J. Phys. C: Solid State Phys. **9**, 2081 (1976).
118. M.E. Zhitomirsky and I.A. Zaliznyak. Phys. Rev. B: Condens. Matter, **53**, 3428 (1996).
119. Z. Tun, W.J.L. Buyers, R.L. Armstrong, K. Hirakawa, and B.Briat. Phys. Rev. B: Condens. Matter, **42**,4677 (1990).
120. I. Affleck. J. Phys.: Condens. Matter, **1**, 3047 (1989); I. Affleck and G.F. Wellman. Phys. Rev. B: Condens. Matter, **46**, 8934 (1992).
121. I.A. Zaliznyak. Solid State Commun. **84**, 573 (1992).
122. M.L. Plumer, K. Hood, and A. Caillé. Phys. Rev. Lett. **60**, 45 (1988).
123. H. Kawamura, A. Caillé, and M.L. Plumer. Phys. Rev. B: Condens. Matter, **41**, 4416 (1990).
124. H. Kawamura. Phys. Rev. B: Condens. Matter, **47**, 3415 (1993).
125. M. Enderle, R. Schneider, Y. Matsuoka, and K. Kakurai. Physica B, **234**, 554 (1997).
126. H. Weber, D. Beckmann, J. Wosnitza, H. v. Löhneysen, and D. Visser. Intern. J. Modern Phys. B, **9**, 1387 (1995).
127. H. Tanaka, H. Nakano, and S.Matsuno. J. Phys. Soc. Jpn. **63**, 3169 (1994).
128. A.N. Bazhan, I.A. Zaliznyak, D.V. Nikiforov, O.A. Petrenko, S.V. Petrov, and L.A. Prozorova. Sov. Phys. JETP, **76**, 342 (1993).
129. T. Kato, T. Ishii, Y. Ajiro, T. Asano, and S. Kawano. J. Phys. Soc. Jpn. **62**, 3384 (1993).
130. O.A. Petrenko, M.F. Collins, C.V. Stager, B.F. Collier, and Z. Tun. J. Appl. Phys. **79**, 6614 (1996).
131. M.L. Plumer, A. Caillé, and K. Hood. Phys. Rev. B: Condens. Matter, **39**, 4489 (1989).
132. M. Kerszberg and D. Mukamel. Phys. Rev. B: Condens. Matter, **18**, 6283 (1978).
133. J.A. Oyedele and M.F. Collins. Can. J. Phys. **56**, 1482 (1978).
134. A.V. Chubukov. J. Phys. C: Solid State Phys. **21**, L441 (1988).
135. T.E. Mason, M.F. Collins, and B.D. Gaulin. J. Appl. Phys. **67**, 5421 (1990).
136. S.I. Abarzhi. Sov. Phys. JETP, **76**, 676 (1993).
137. T.E. Mason, C.V. Stager, B.D. Gaulin and M.F. Collins. Phys. Rev. B: Condens. Matter, **42**, 2715 (1990).
138. T.E. Mason, Y.S. Yang, M.F. Collins, B.D. Gaulin, K.N. Clausen, and A. Harrison. J. Magn. Magn. Mater. **104–107**, 197 (1992)
139. T. Goto, T. Inami, and Y. Ajiro. J. Phys. Soc. Jpn. **59**, 2328 (1990).

140. B.Ya. Kotyuzhanskii and D.V. Nikiforov. J. Phys. Condens. Matter, **3**, 385 (1991).
141. S.I. Abarzhi, A.N. Bazhan, L.A. Prozorova, and I.A. Zaliznyak. J. Phys.: Condens. Matter, **4**, 3307 (1992).
142. I.A. Zaliznyak, L.A. Prozorova, and S.V. Petrov. Sov. Phys. JETP, **70**, 203 (1990).
143. P. Santini, Z. Domanski, J. Dong, and P. Erdos. Phys. Rev. B: Condens. Matter, **54**, 6327 (1996).
144. M.L. Plumer and A. Mailhot. Phys. Rev. B: Condens. Matter, **50**, 16 113 (1994).
145. E.H. Boubcheur, D. Loison, and H.T. Diep. Phys. Rev. B: Condens. Matter, **54**, 4165 (1996).
146. M.L. Plumer and A. Mailhot. J. Phys. Condens. Matter, **9**, L165 (1997).
147. T.E. Mason, M.F. Collins, and B.D. Gaulin. J. Phys. C: Solid State Phys. **20**, L945 (1987).
148. Y. Ajiro, T. Nakashima, Y. Unno, H. Kadowaki, M. Mekata, and N. Achiwa. J. Phys. Soc. Jpn. **57**, 2648 (1988).
149. T. Kato, T. Asano, Y. Ajiro, S. Kawano, T. Ishii, and K. Iio. Physica B, **213&214**, 182 (1995).
150. H. Kadowaki, S.M. Shapiro, T. Inami, and Y. Ajiro. J. Phys. Soc. Jpn. **57**, 2640 (1988).
151. J. Wang, D.P. Belanger, and B.D. Gaulin. Phys. Rev. Lett. **66**, 3195 (1991).
152. R. Deutschmann, H. von Lohneysen, J. Wosnitza, R.K. Kremer, and D. Visser. Euro. Phys. Lett. **17**, 637 (1992).
153. M. Eibschütz, G.R. Davidson, and D.E. Cox. AIP Conf. Proc. **18**, 386 (1973).
154. H. Kawamura, Prog. Theor. Phys. Suppl. **101**, 545 (1990).
155. W. Zhang, W.M. Saslow, and M. Gabay. Phys. Rev. B: Condens. Matter, **44**, 5129 (1991); W. Zhang, W.M. Saslow, M. Gabay, and M.Benakli. Phys. Rev. B: Condens. Matter, **48**, 10 204 (1993).
156. M.L. Plumer, A. Caillé, and H. Kawamura. Phys. Rev. B: Condens. Matter, **44**, 4461 (1991)
157. M.E. Zhitomirsky, O.A. Petrenko, and L.A. Prozorova. Phys. Rev. B: Condens. Matter, **52**, 3511 (1995).
158. D. Visser, G.C. Verschoor, and D.J.W. Ijdo. Acta. Crystallogr. **B36**, 28 (1980).
159. H. von Fink and H.-J. Seifert. Acta Crystallogr. **B38**, 912 (1982).
160. K. Machida, T. Mitsui, T. Kato, and K. Iio. Solid State Commun. **91**, 17 (1994).
161. O.A. Petrenko, M.A. Lumsden, M. Lumsden, and M.F. Collins. J. Phys.: Condens. Matter, **8**, 10899 (1996)
162. I.M. Vitebskii, O.A. Petrenko, S.V. Petrov, and L.A. Prozorova. Sov. Phys. JETP, **76**, 178 (1993).
163. M.E. Zhitomirsky. Phys. Rev. B: Condens. Matter, **54**, 353 (1996).
164. S.E. Nagler, W.J.L. Buyers, R.L. Armstrong, and B. Briat. Phys. Rev. B: Condens. Matter, **27**, 1784 (1983).
165. G.H. Wannier. Phys. Rev. **79**, 357 (1950).
166. U. Tellenbach and H. Arend. J. Phys C: Solid State Phys. **10**, 1311 (1977).
167. H. Yoshizawa and K. Hirakawa. J. Phys. Soc. Jpn. **46**, 4487 (1979).
168. H. Yoshizawa, K. Hirakawa, S.K. Satiya, and G. Shirane. Phys. Rev. B: Condens. Matter, **23**, 2298 (1981)
169. H. Yoshizawa, J.D. Axe, and G. Shirane. Solid State Commun. **38**, 241 (1981).
170. H. Hori, H. Mikami, M. Date, Y. Ajiro, and N. Mori. J. Magn. Magn. Mater. **104–107**, 815 (1992).
171. J.B. Ward, V.H. McCann, Q.A. Pankhurst, W.L. Hassett, and D.C. Price. J. Phys. C: Solid State Phys. **20**, 1689 (1987).
172. M. Mekata, S. Okamoto, S. Onoe, S. Mitsuda, and H.Yoshizawa. J. Magn. Magn. Mater. **90&91**, 267 (1990).
173. K. Amaya, H. Hori, I. Shiozaki, M. Date, M. Ishizuka, T. Sakakibari, T. Goto, N. Miura, H. Kikuchi, and Y. Ajiro. J. Phys. Soc. Jpn. **59**, 1810 (1990).
174. S. Bocquet, J.B. Ward, and V.H. McCann. J. Phys. C: Solid State Phys. **21**, 367 (1988).
175. D.J. Lockwood, I.W. Johnstone, H.J. Labbe, and B. Briat. J. Phys. C: Solid State Phys. **16**, 6451 (1983).
176. S.E. Nagler, W.J.L. Buyers, R.L. Armstrong, and B. Briat. Phys. Rev. B: Condens. Matter, **28**, 3873 (1983).
177. R. Rogge. Ph.D. thesis, McMaster University, Hamilton, Ont., Canada 1994.
178. A. Farkas, B.D. Gaulin, Z. Tun, and B. Briat. J. Appl. Phys. **69**, 6167 (1991).
179. J.P. Boucher, L.P. Regnault, J. Rossat-Mignod, Y. Henry, J. Bouillot, and W.G. .Stirling. Phys. Rev. B: Condens. Matter, **31**, 3015 (1985).
180. J. Wang, D.P. Belanger, and B.D.Gaulin. Phys. Rev. B: Condens. Matter, **49**, 12299 (1994).
181. A.N. Berker, G.S. Grest, C.M. Soukoulis, D. Blankschtein, and M. Ma. J. Appl. Phys. **55**, 2416 (1984);

D. Blankschtein, M. Ma, A.N. Berker, G.S. Grest, and C.M. Soukoulis. Phys. Rev. B: Condens. Matter, **29**, 5250 (1984).
182. M.L. Plumer, A. Caillé, and K. Hood. Phys. Rev. B: Condens. Matter, **40**, 4958 (1989).
183. M. Melamud, H. Pinto, J. Makovsky, and H. Shaked. Phys. Status Solidi B, **63** 699 (1974).
184. T. Kurata and H. Kawamura. J. Phys. Soc. Jpn. **64**, 232 (1995).
185. S.N. Coppersmith. Phys. Rev. B: Condens. Matter, **32**, 1584 (1985).
186. T. Kohmoto, T. Goto, S. Maegawa, N. Fujiwara, Y. Fukuda, N. Kunitomo, and M. Mekata. Phys. Rev. B: Condens. Matter, **52**, 12526 (1995).
187. F. Matsubara and S. Ikeda. Phys. Rev. B: Condens. Matter, **28**, 4064 (1983).
188. F. Matsubara and S. Inawashiro. J. Phys. Soc. Jpn. **53**, 4373 (1984).
189. F. Matsubara and S. Inawashiro. J. Phys. Soc. Jpn. **56**, 2666 (1987).
190. O. Heinonen and R.G. Petschek. Phys. Rev. B: Condens. Matter, **40**, 9052 (1989).
191. A. Bunker, B.D. Gaulin, and C. Kallin. Phys. Rev. B: Condens. Matter, **48**, 15861 (1993); Phys. Rev. B: Condens. Matter, **52**, 1415 (1995).
192. M.L. Plumer and A. Mailhot. Phys. Rev. B: Condens. Matter, **52**, 1411 (1995).
193. M.L. Plumer, A. Mailhot, R. Ducharme, A. Caillé, and H.T. Diep. Phys. Rev. B: Condens. Matter, **47**, 14 312 (1993).
194. W.J.L. Buyers, M.L. Hogan, R.L. Armstrong, and B. Briat. Phys. Rev. B: Condens. Matter, **33**, 1727 (1986).
195. Z. Tun, B.D. Gaulin, R. B. Rogge, and B. Briat. J. Magn. Magn. Mater. **104–107**, 1045 (1992).
196. C.N. Yang and C.P. Yang. Phys. Rev. **151**, 258 (1966).
197. A. Harrison, C.V. Stager, and D. Visser. J. Appl. Phys. **69**, 5998 (1991).
198. D. Visser and A. Harrison. J. Magn. Magn. Mater. **116**, 80 (1992).
199. D. Visser and A. Harrison. J. Phys. Colloque, **C8**, 1467 (1988).
200. M. Eibschütz, M.E. Lines, and R.C. Sherwood. Phys. Rev. B: Condens. Matter, **11**, 4595 (1975).
201. M. Steiner, K. Kakurai, W. Knop, B. Dorner, R. Pynn, U. Happek, P. Day, and G. McLeen. Solid State Commun. **38**, 1179 (1981).
202. W. Knop, M. Steiner, and P. Day. J. Magn. Magn. Mater. **31–34**, 1033 (1983).
203. In ref.29 cited as: K. Takeda et al. Private communication about a specific heat measurements on $CsFeCl_3$.
204. In ref.228 cited as: D.P. Dickson, private communication. 1981.
205. P.A. Montano, H. Shechter, E. Cohen, and J. Makovsky. Phys. Rev. B: Condens. Matter, **9**, 1066 (1974).
206. B. Schmid, B. Dorner, D. Petitgrand, L.P. Regnault, and M. Steiner. Z. Phys. B, **95**, 13 (1994).
207. M. Chiba, Y. Ajiro, K. Adachi, and T. Morimoto. J. Phys. Soc. Jpn. **57**, 3178 (1988); J. Phys. Colloque C8, **49**, 1445 (1988).
208. N. Suzuki and J. Makino. J. Phys. Soc. Jpn. **64**, 2166 (1995).
209. B. Schmid, B. Dorner, D. Visser, and M. Steiner. Z. Phys. B: Condens. Matter, **86**, 257 (1992); J. Magn. Magn. Mater. **104–107**, 771 (1992).
210. B. Dorner, D. Visser, U. Steigenberger, K. Kakurai, and M. Steiner. Physica B, **156&157**, 263 (1989).
211. D. Visser, B. Dorner, and M. Steiner. Physica B, **174**, 25 (1991).
212. G.R. Davidson, M. Eibschutz, D.E. Cox, and V.J. Minkiewicz. AIP Conf. Proc. **5**, 436 (1971).
213. N. Suzuki. J. Phys. Soc. Jpn. **50**, 2931 (1981).
214. M.E. Lines and M. Eibschüts. Phys. Rev. B: Solid State, **11**, 4583 (1975).
215. K. Adachi, K. Takeda, F. Matsubara, M. Mekata, and T. Haseda. J. Phys. Soc. Jpn. **52**, 2202 (1983).
216. A. Harrison and D.Visser. Phys. Lett. **137A**, 79 (1989).
217. Y. Takeda, M. Shimada, F. Kanamura, and M. Koizumi. J. Phys. Soc. Jpn. **37**, 276 (1974).
218. N. Papanicolaou and P. Spathis. J. Phys.: Condens. Matter, **1**, 5555 (1989).
219. N. Papanicolaou and P. Spathis. J. Phys.: Condens. Matter, **2**, 6575 (1990).
220. P.-A. Lindgard and B. Schmid. Phys. Rev. B: Condens. Matter, **48**, 13 636 (1993).
221. W.-M. Liu and B.-L. Zhou. Z. Phys. B: Condens. Matter, **93**, 395 (1994).
222. B. Dorner, D. Visser, and M. Steiner. Z. Phys. B: Condens. Matter, **81**, 75 (1990).
223. T. Mitsui, K. Machida, T. Kato, and K. Iio. J. Phys. Soc. Jpn. **63**, 839, (1994).
224. H. Shiba. Solid State Commun. **41**, 511 (1982).
225. H. Shiba and N.Suzuki. J. Phys. Soc. Jpn. **51**, 3488 (1982).

226. T. Haseda, N. Wada, M. Hata, and K.Amaya. Physica B, **108**, 841 (1981).
227. T. Tsuboi, M. Chiba, H. Hori, I. Shiozaki, and M. Date. J. Phys. Colloque C8, **49**, 1443 (1988).
228. J.A. Baines, C.E. Johnson, and M.F. Thomas. J. Phys. C: Solid State Phys. **16**, 3579 (1983).
229. P.-A. Lindgard. J. Magn. Magn. Mater. **54–57**, 1227 (1986).
230. H. Ohta, N. Makita, K. Yoshida, T. Nanba, and M. Motokawa. Int. J. Infrared Millimeter Waves, **13**, 457 (1992).
231. H. Ohta, D. Donnelly, and M. Motokawa. J. Magn. Magn. Mater. **104–107**, 777 (1992).
232. T. Goto, S. Maegawa, and T. Kawai. J. Phys. Soc. Jpn. **55**, 1066 (1986).
233. N. Wada, K. Ubukoshi, and K. Hirakawa. J. Phys. Soc. Jpn. **51**, 2833 (1982).
234. N. Wada, K. Sumiyoshi, T. Watanabe, and K. Amaya. J. Phys. Soc. Jpn. **52**, 1893 (1983).
235. B. Dorner, B. Schmid, K. Kakurai and D. Petitgrand. Can. J. Phys. **73**, 800 (1995).
236. K. Amaya, M. Ishizuka, T. Nakagawa, S. Saratani, T. Sakakibara, S. Takeyama, K. Nakao, T. Goto, N. Miura, Y. Unno, and Y. Ajiro. J. Phys. Soc. Jpn. **57**, 38 (1988).
237. N. Achiwa. J. Phys. Soc. Jpn. **27**, 561 (1969).
238. P.A. Montano, E. Cohen, H. Shechter, and J. Makovsky. Phys. Rev. B: Solid State, **7**, 1180 (1973).
239. M.E. Lines. Phys. Rev. B: Solid State, **11**, 1134 (1975).
240. N. Suzuki. J. Phys. Soc. Jpn. **45**, 1791 (1978).
241. N. Suzuki. J. Phys. Soc. Jpn. **52**, 3907 (1983).
242. N. Suzuki. J. Phys. Soc. Jpn. **52**, 1002 (1983).
243. A.W. Schlueter, R. A. Jacobson, and R.E. Rundle. Inorg. Chem. **5**, 277 (1966).
244. C.J. Kroese, W.J.A. Maaskant, and G.C. Verschoor. Acta Crystallogr. B, **30**, 1053 (1974).
245. M. Mekata, Y. Ajiro, T. Sugino, A. Oohara, K. Ohara, S. Yusada, Y. Oohara, and H. Yoshizawa. J. Magn. Magn. Mater. **140–144**, 1987 (1995).
246. H. Tanaka, K. Iio, and K. Nagata. J. Phys. Soc. Jpn. **54**, 4345 (1985).
247. N. Stuesser, U. Schotte, K.D. Schotte, and X. Hu. Physica B, **213–214**, 164 (1995).
248. E. Rastelli and A. Tassi. Z. Phys. B, **94**, 139 (1994); **94**, 234 (1994).
249. E.P. Stefanovskii, and A.L. Sukstanskii. JETP, **77**, 628 (1993).
250. H. Ohta, S. Imagawa, M. Motokawa, and H.Tanaka. J. Phys. Soc. Jpn. **62**, 3011 (1993).
251. H. Nojiri, Y. Tokunaga, and M. Motakawa. J. Phys. (Paris) Suppl. C8, **49**, 1459 (1988).
252. M. Chiba, Y. Ajiro, and T. Morimoto. Physica B, **211**, 196 (1995).
253. T. Nikuni and H. Shiba. J. Phys. Soc. Jpn. **62**, 3268 (1993). 239
254. N.V. Fedoseeva, R.S. Gekht, T.A. Velikanova, and A.D.Balaev. JETP Lett. **41**, 406 (1985).
255. R.S. Gekht, N.V. Fedoseeva, V.A. Dolina, and A.D. Belaev. Phys. Status Solidi, **155**, 639 (1989).
256. H. Weber, T. Werner, J. Wosnitza. H. v. Löhneysen, and U. Schotte. Phys. Rev. B: Condens. Matter, **54**, 15 924 (1996).
257. A.E. Jacobs, T. Nikuni, and H. Shiba. J. Phys. Soc. Jpn. **62**, 4066 (1993).
258. T. Ohyama and A.E. Jacobs. Phys. Rev. B: Condens. Matter, **52**, 4389 (1995).
259. D. Babel. Z. Anorg. Allgem. Chem. **369**, 117 (1969).
260. K. Kakurai, R. Pynn, B. Dorner, and M. Steiner. J. Phys. C: Solid State Phys. **17**, L123 (1984).
261. M. Steiner. Solid State Commun. **11**, 73 (1972).
262. C. Scherer and Y. Barjhoux. Phys. Status Solidi B, **80**, 313 (1977).
263. N. Suzuki. J. Phys. Soc. Jpn. **52**, 3199 (1983).
264. Y. Trudeau and M.L. Plumer. Phys. Rev. B: Condens. Matter, **51**, 5868 (1995).
265. M.L. Plumer and A.Caillé. Phys. Rev. B: Condens. Matter, **37**, 7712 (1988).
266. M. Steiner and J.K. Kjems. J. Phys. C: Solid State Phys. **10**, 2665 (1977).
267. M. Steiner. Phase Transitions, **1**, 269 (1980).
268. J.V. Lebesque, J. Snel, and J.J. Smit. Solid State Commun. **13**, 371 (1973).
269. C. Dupas and J-P. Renard. J. Phys. C: Solid State Phys. **10**, 5957 (1977).
270. H. Yamazaki, E. Soares, H. Panepucci, and Y. Morishige. J. Phys. Soc. Jpn. **47**, 1464 (1979).
271. B. Lussier and M. Poirier. Phys. Rev. B: Condens. Matter, **48**, 6199 (1993).
272. M. Steiner and H. Dachs. Solid State Commun. **14**, 841 (1974).
273. J.M. Lovelock and J. Villain. J. Phys. Lett. (Paris), **38**, L77 (1977).
274. D. Loison and H.T. Diep. J. Appl. Phys. **73**, 5642 (1993).
275. C.L. Henley. Phys. Rev. Lett. **62**, 2056 (1989).

276. M. Mekata, T. Tatsumi, T. Nakashima, K. Adachi, and Y. Ajiro. J. Phys. Soc. Jpn. **56**, 4544 (1987).
277. M.E. Zhitomirsky, O.A. Petrenko, S.V. Petrov, L.A. Prozorova, and S.S. Sosin. Sov. Phys. JETP, **81**, 185 (1995).
278. H. Yamazaki, K. Minami, and K. Katsumata. J. Phys.: Condens. Matter, **8**, 8407 (1996).
279. A. Harrison and D. Visser. J. Phys.: Condens. Matter, **2**, 10487 (1990).
280. Y. Oohara and K. Iio. J. Phys. Soc. Jpn. **63**, 4597 (1994).
281. J. Takeuchi, T. Wada, I. Hiromitsu, and T. Ito. Solid State Commun. **87**, 899 (1993).
282. Y. Trudeau, M.L. Plumer, M. Poirier, and J. Takeuchi. Phys. Rev. B: Condens. Matter, **52**, 378 (1995).
283. H. Tanaka, T. Hasegawa, and K. Nagata. J. Phys. Soc. Jpn. **62**, 4053 (1993).
284. A. Harrison, D. Visser, P. Day, W. Knop, and M. Steiner. J. Phys. C: Solid State Phys. **19**, 6811 (1986).
285. A. Harrison and D. Visser. J. Phys.: Condens. Matter, **1**, 733 (1989).
286. A. Harrison. J. Phys.: Condens. Matter, **1**, 6695 (1989).
287. A.P. Ramirez, G.P. Espinosa, and A.S.Cooper. Phys. Rev. Lett. **64**, 2070 (1990).
288. S. Hov, H. Bratsberg and A.T. Skjeltorp. J. Magn. Magn. Mater. **15–18** 1980 (1980).
289. P. Schiffer, A.P. Ramirez, D.A. Huse, P.L. Gammel, U. Yaron, D.J. Bishop, and A.J. Valentino. Phys. Rev. Lett. **74**, 2379 (1995).